

INDUCTIVE STORAGE SWITCH STUDY

Dr. R. W. Waniek
Dr. H. P. Furth
D. M. Fitzgerald, et al
Advanced Kinetics, Inc

Distribution of this document is unlimited

FOREWORD

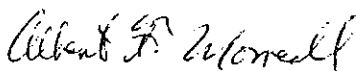
This report was prepared by Advanced Kinetics, Inc., 1231 Victoria Street, Costa Mesa, California, under Contract AF30(602)-3512 (Project 4506, Task 450603). The following personnel contributed to the work presented in this technical report:

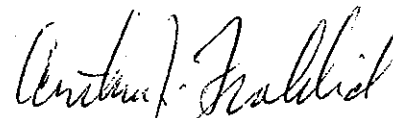
Dr. R. W. Waniek
Dr. H. P. Furth
Mr. D. M. Fitzgerald
Mr. R. T. Givens
Mr. W. Chen

Mr. M. J. Dowd
Mr. R. L. Mollet
Mr. J. G. Koscelnik
Mr. T. H. Vannus
Mr. H. J. Gilsdorf

Mr. Albert F. Morreall (EMATP) was the Rome Air Development Centers project engineer.

This technical report has been reviewed and is approved.


Approved: ALBERT F. MORREALL
Project Engineer


Approved: THOMAS S. BOND, Jr.
Colonel, USAF
Chief, Surveillance & Control Division

FOR THE COMMANDER:


IRVING J. GABELMAN
Chief, Advanced Studies Group

ABSTRACT

The problems encountered when discharging an inductive storage device into a load are discussed in detail. Experiments with a switch using a liquid metal to solid metal contact resulted in electrode erosion which could not be prevented. This led to the exclusive use of liquid electrodes which are self-healing. A variety of switch configurations were devised and tested including two types of vertical flow interrupters. Data from these tests which were conducted with both mercury and liquid sodium as the switching medium is presented.

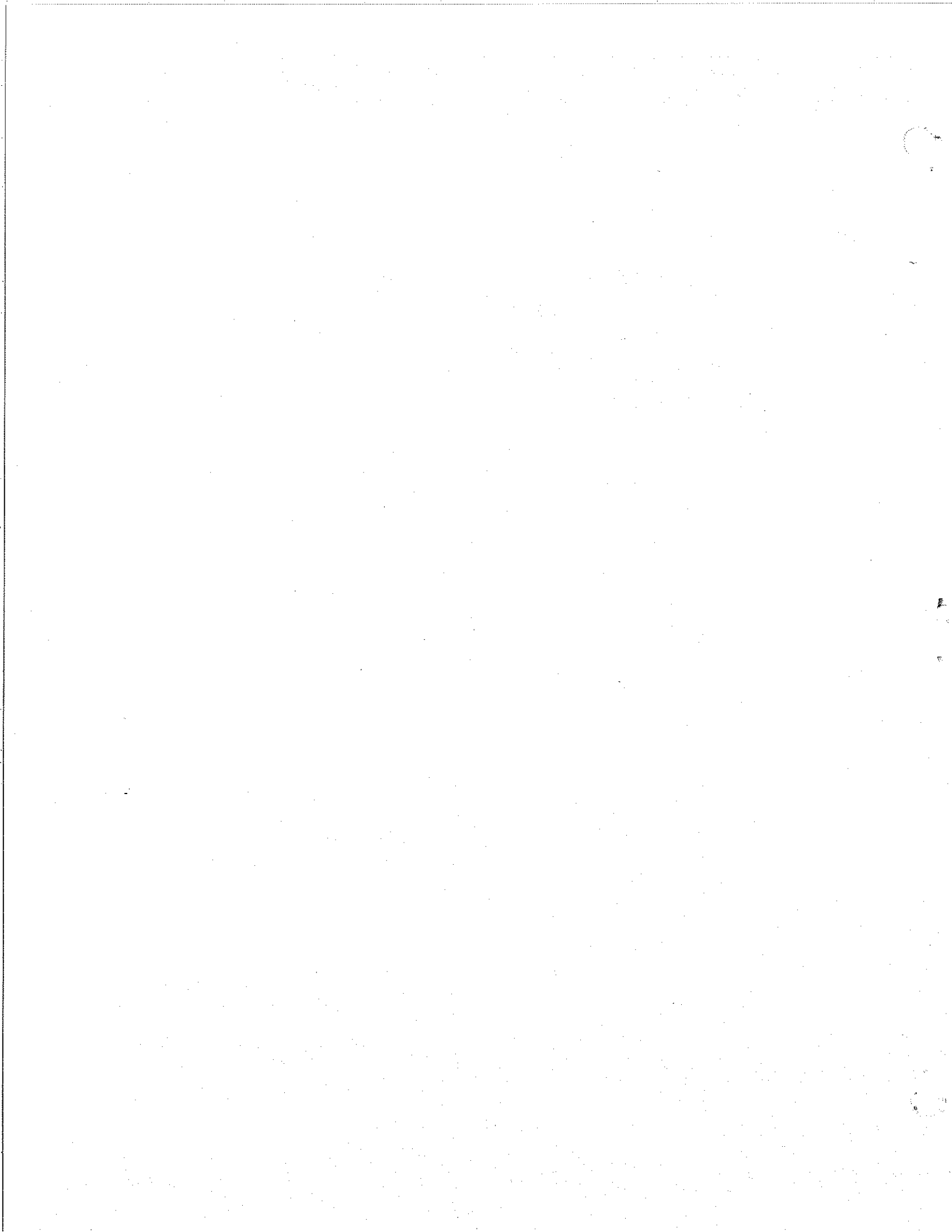


TABLE OF CONTENTS

	Page
I) THEORETICAL AND ANALYTICAL CONSIDERATIONS	
A) ANALYSIS OF THE INDUCTIVE STORAGE SWITCHING PROBLEM.....	1
1) The Ideal Circuit	1
2) Experimental Circuit (IND-1)	6
B) STABILITY OF A LIQUID METAL COLUMN	12
C) STABILITY OF A TUBULAR LIQUID METAL FLOW	16
D) COMPARISON OF LIQUID METALS FOR FLUID-TO-FLUID INTERRUPTION	20
II) EXPERIMENTAL PROGRAM	
A) INTRODUCTION	23
B) SINGLE-CELL MULTI-SHOT INTERRUPTER (MSI-3)	24
1) Design Considerations	24
2) Operational Results with Mercury	25
3) Operational Results with Sodium	32
C) TRIPLE-CELL MULTI-SHOT INTERRUPTER (MSI-4)	38
1) Design Considerations	38
2) Results with the MSI-4P	40
3) Results with the MSI-4T	43
D) COLUMNAR VERTICAL FLOW INTERRUPTER (CVFI)	47
III) CONCLUSIONS	54

APPENDIX - Figures 1 through 48 follow text.

LIST OF ILLUSTRATIONS

(Following text)

- Fig. 1: Coaxial Configuration Incorporating the Flow of Liquid Metal
- Fig. 2: Perturbations due to the Passage of Current through a Flowing Liquid
- Fig. 3: Tubular Flow of Liquid Metal
- Fig. 4: Breakup of a Tubular Liquid Metal Flow by means of an Auxiliary Circuit
- Fig. 5: Density as a Function of Temperature for Lithium
- Fig. 6: Density as a Function of Temperature for Sodium
- Fig. 7: Density as a Function of Temperature for Potassium
- Fig. 8: Density as a Function of Temperature for Sodium-Potassium Alloy (44K - 56 Na)
- Fig. 9: Density as a Function of Temperature for Sodium Potassium Alloy (78K - 22 Na)
- Fig. 10: Density as a Function of Temperature for Gallium
- Fig. 11: Density as a Function of Temperature for Mercury
- Fig. 12: Electrical Resistivity as a Function of Temperature - Lithium
- Fig. 13: Electrical Resistivity as a Function of Temperature for Sodium
- Fig. 14: Electrical Resistivity as a Function of Temperature - Potassium
- Fig. 15: Electrical Resistivity as a Function of Temperature for Sodium-Potassium Alloy
(44K - 56 Na)
- Fig. 16: Electrical Resistivity as a Function of Temperature for Sodium-Potassium Alloy
(78K - 22 Na)
- Fig. 17: Electrical Resistivity as a Function of Temperature - Mercury
- Fig. 18: Cutaway View of the MSI-3
- Fig. 19: The MSI-3 Testing Circuitry

LIST OF ILLUSTRATIONS - Continued

- Fig. 20: % of Perfect Transfer vs Inductor Current Using MSI-3 Self-Interruption Mode with Atmospheric Pressure Nitrogen in the Switching Chamber
- Fig. 21: Dwell Time vs Peak Inductor Current Using MSI-3 Self-Interruption Mode with Atmospheric Pressure Nitrogen in Switching Chamber
- Fig. 22: Arc Duration vs Peak Inductor Current Using MSI-3 Self-Interruption Mode with Atmospheric Pressure Nitrogen in Switching Chamber
- Fig. 23: % of Energy Transferred to Load vs Total Stored Energy Using MSI-3 Self-Interruption Mode with Atmospheric Pressure Nitrogen in Switching Chamber
- Fig. 24: % of Perfect Transfer vs Total Stored Energy Using MSI-3 Self-Interruption Mode with Atmospheric Pressure Nitrogen in the Switching Chamber
- Fig. 25: Dwell Time vs Pressure Using MSI-3 Self-Interruption Mode with Nitrogen Gas at Various Pressures in Switching Chamber
- Fig. 26: % of Energy Transfer vs Pressure Using MSI-3 Self-Interruption Mode with Nitrogen Gas at Various Pressures in Switching Chamber
- Fig. 27: % of Perfect Transfer vs Pressure Using MSI-3 Powered-Interruption Mode and Pressurized Nitrogen in Switching Chamber (Bank Energy 900 joules)
- Fig. 28: % of Perfect Transfer vs Pressure Using MSI-3 Powered-Interruption Mode and Pressurized Nitrogen in Switching Chamber (Bank Energy 1600 joules)
- Fig. 29: % of Maximum Voltage Across Load vs Pressure for Two Bank Energies Using MSI-3 Powered-Interruption Mode and Pressurized Nitrogen in Switching Chamber
- Fig. 30: MSI-3 Teflon Insert and Heating Elements for Work with Liquid Sodium
- Fig. 31: % of Perfect Transfer vs Pressure for Three Peak Inductor Currents Using MSI-3 Self-Interruption Mode and Pressurized Nitrogen in Switching Chamber
- Fig. 32: % of Perfect Transfer vs Pressure for Three Peak Inductor Currents Using MSI-3 Self-Interruption Mode and Pressurized Argon in Switching Chamber
- Fig. 33: % of Perfect Transfer vs Maximum Inductor Current for Three Pressures Using MSI-3 Self-Interruption Mode and Pressurized Nitrogen in Switching Chamber

LIST OF ILLUSTRATIONS - Continued

- Fig. 34: % of Perfect Transfer vs Maximum Inductor Current for Three Pressures Using MSI-3 Self-Interruption Mode and Pressurized Argon in Switching Chamber
- Fig. 35: MSI-4T Teflon Insert
- Fig. 36: MSI-4P Teflon Insert
- Fig. 37: Cross-sectional Diagram of the MSI-4T
- Fig. 38: % of Perfect Transfer vs Pressure for Various Bank Energies Using MSI-4P Powered-Interruption Mode and Pressurized Nitrogen in Switching Chamber
- Fig. 39: The Columnar Vertical Flow Interrupter (CVFI)
- Fig. 40: Circuitry for Preliminary Testing of the CVFI
- Fig. 41: Voltage Across 1 Megohm Resistor
- Fig. 42: Example of Self-Interruption and Powered-Interruption with Pancake Type Coil
- Fig. 43: Horizontal Component of B-Field of the Helmholtz Configuration taken along Axis of the Coils
- Fig. 44: The C-90 Coil
- Fig. 45: Field Geometry Produced by the C-90 Coil
- Fig. 46: B-Field Pickup in Gap of C-90 Coil
- Fig. 47: Interruption Produced by Self-Interruption and an Energized C-90 Coil
- Fig. 48: Double C-Core Experimental Configuration showing the Forces Exerted on the Mercury Column

EVALUATION

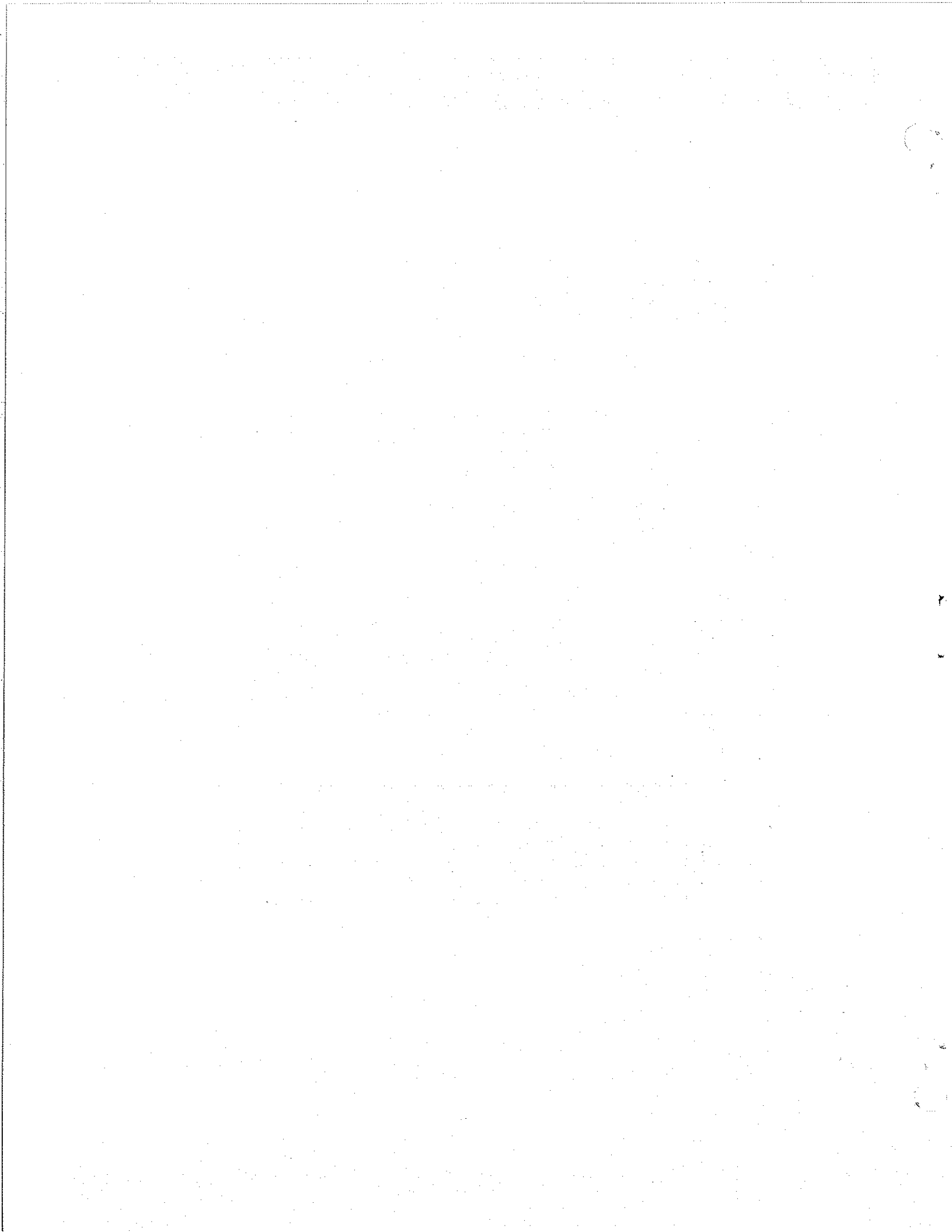
This effort was a continuation of an investigation of switching techniques for use with inductive energy storage systems in pulsed modulator operation. The major objective was the development of a high current passing switch which could be opened quickly and completely, thereby permitting maximum transfer of energy from the storage inductor to the load. Operation at pulse widths, repetition rates and pulse energies compatible with long range radar systems was desired.

The inherent tendency of metallic switch contacts to erode when opened under high currents led to the exclusive use of self healing liquid metal electrodes. Several different switch configurations were developed which could be activated with a pulsed magnetic field. Both mercury and liquid sodium were employed under a variety of pressurized conditions in an effort to optimize control and minimize losses. The most promising design appeared to be the vertical liquid column switch where pulse widths and repetition rates were simple to control and heat dissipation offered no serious problem.

Although the amount of energy which could be transferred and the efficiencies attained were promising, the difficulty in obtaining high voltage holdoff appears to be insurmountable with the devices considered. This problem presents a serious limitation to the use of inductive storage systems in long range radar application. Other areas of endeavor, (exploding wires, etc.), would benefit more from this work at this time. In view of this, RADC will not continue this investigation until device concepts can be developed which show promise of solving the voltage holdoff problem.

This program was one of a series of efforts to advance the state-of-the-art of high power modulator switching techniques. This and related programs have indicated that mechanical rotating machines are most suitable for very long pulse widths and capacitive energy storage devices for very small pulse widths. Inductive storage systems offer many advantages in the intermediate pulse width range but the switching problem has prevented their use in high power long range systems.

Albert F. Morreall
ALBERT F. MORREALL
Project Engineer

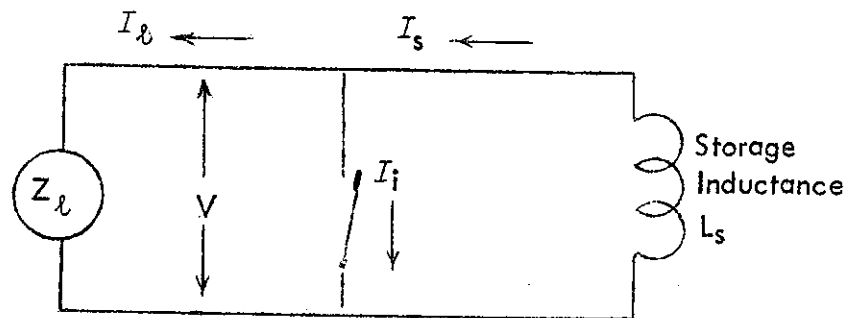


1) THEORETICAL AND ANALYTICAL CONSIDERATIONS

A) ANALYSIS OF THE INDUCTIVE STORAGE SWITCHING PROBLEM

1) The Ideal Circuit

We treat here a generalized ideal circuit for discharging an inductive storage device into a load. The results obtained will then be applied to a real circuit used during the course of the experiments conducted in this program.



The storage inductance and the interrupter switch (when closed) are assumed to have no internal resistance. Therefore, prior to the beginning of the switching process, the current circulates through the inductor and interrupter switch with no losses. We are confining ourselves here to a dissipative type of interrupter switch and to a purely resistive load which may be slowly time-varying in that the resistance depends upon the temperature; the temperature depends upon the energy previously dissipated in the

load, with the energy being a function of time.

At time $t = 0$, as the interrupting process begins, we have

$$I_l = 0 \quad (1)$$

$$I_i = I_s = I_0$$

while, at time $t = \tau$, when the interrupter is fully open, we have

$$I_i = 0 \quad (2)$$

$$I_l = I_s = I_1$$

During the interval $0 \leq t \leq \tau$ the amounts of energy that go into the interrupter and load, respectively, are given by

$$E_i = \int_0^{\tau} V I_i dt \quad (3)$$

and

$$E_l = \int_0^{\tau} V I_l dt \quad (4)$$

where the sum of these must be equal to the energy lost by the inductor during this time

$$\int_0^{\tau} V I_i dt + \int_0^{\tau} V I_l dt = \frac{1}{2} L_s I_0^2 - \frac{1}{2} L_s I_1^2 \quad (5)$$

Since we are dealing with a purely resistive load the voltage V increases

from zero at $t = 0$ to its maximum value

$$V_{\max} = I_1 R_l \quad (6)$$

at $t = \tau$ at which point the interrupter is an open circuit.

Using Kirchhoff's law ($I_s = I_i + I_l$) we can write

$$\int_0^{\tau} V I_i dt + \int_0^{\tau} V I_l dt = \int_0^{\tau} V I_s dt \quad (7)$$

where we know that I_s decreases from I_0 to I_1 during the time τ . Then

$$\int_0^{\tau} V I_s dt < I_1 R_l I_0 \tau \quad (8)$$

where we have replaced the functions in the integral by their maximum values outside the integral.

Assuming for the present that

$$\int_0^{\tau} V I_i dt \gg \int_0^{\tau} V I_l dt \quad (9)$$

we then find that the efficiency ϵ is given by

$$\epsilon = \frac{\frac{1}{2} L_s I_0^2 - (\frac{1}{2} L_s I_0^2 - \frac{1}{2} L_s I_1^2)}{\frac{1}{2} L_s I_0^2} \quad (10)$$

Now by using Eqs. (5), (7), and (8), we have

$$\epsilon > \frac{\frac{1}{2} L_s I_0^2 - I_1 I_0 R_l \tau}{\frac{1}{2} L_s I_0^2} = 1 - \tau (2I_1/I_0)(R_l/L_s) \quad (11)$$

and we find that

$$\tau (2I_1/I_0)(R_L/L_S) < (1 - a) \quad (12)$$

insures that $\epsilon > a$, where a is a lower bound of the switching efficiency ($0 \leq a \leq 1$).

Isolating τ in Eq. (12), we have

$$\tau < (1 - a)(L_S/R_L)(I_0/2I_1) \quad (13)$$

and since I_0 is always greater than or equal to I_1 , τ can be expressed as

$$\tau < \frac{1}{2} (1 - a)(L_S/R_L) \quad (14)$$

This restriction on τ is a sufficient condition, although not a necessary one, for the total switching efficiency to be greater than a .

For example, efficiencies greater than .99 could be achieved if

$$\tau < (.005)(L_S/R_L) \quad (15)$$

(i.e., a 5 millisecond interruption and a 1 second L/R time would result in a switching efficiency of more than 99%).

If the switching efficiency during the interval $0 \leq t \leq \tau$ is represented by α , we have

$$\alpha = \int_0^\tau V I_L dt \left[\int_0^\tau V I_I dt + \int_0^\tau V I_L dt \right]^{-1} \quad (16)$$

The energy dissipated in the interrupter switch during this time can be expressed as

$$\int_0^{\tau} V I_i dt = (1 - \alpha) \left(\frac{1}{2} L_s I_0^2 - \frac{1}{2} L_s I_1^2 \right) \quad (17)$$

In this case the total switching efficiency is

$$e = (E_0 - \int_0^{\tau} V I_i dt) E_0^{-1} \quad (18)$$

$$e = \frac{\frac{1}{2} L_s I_0^2 - \left(\frac{1}{2} L_s I_0^2 - \frac{1}{2} L_s I_1^2 \right) (1 - \alpha)}{\frac{1}{2} L_s I_0^2} \quad (19)$$

By proceeding with the calculations as in Eqs. (10) through (13), we find that if

$$\tau < (1 - \alpha)(L_s/R_L)(I_0/2I_1)(1 - \alpha)^{-1} \quad (20)$$

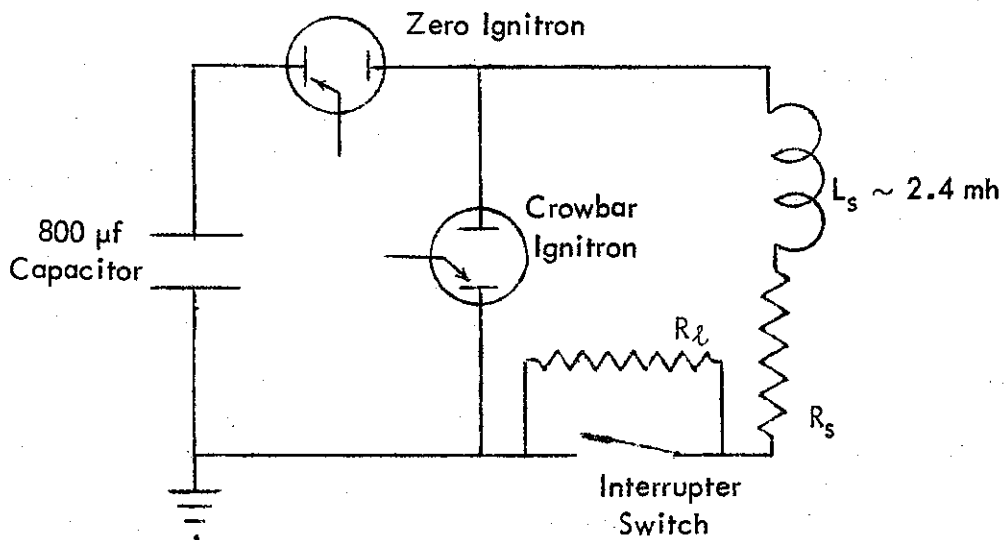
is satisfied, the net switching efficiency must be greater than α for the idealized circuit.

By knowing the complete time-history of the switch impedance, an exact relationship between τ and the switching efficiency could be evolved. However, the difficulties involved in determining the impedance of the high pressure arc in the interrupter switch make this type of approach untenable.

2) Experimental Circuit (IND-1)

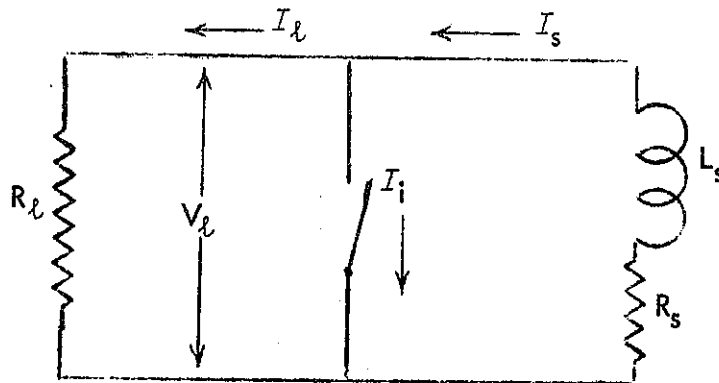
The testing circuit used during the course of these studies is shown schematically below. Charging of the inductor is achieved by triggering the "zero ignitron" while the interrupter switch is in the closed position.

A capacitor is used here rather than a dc charging supply so that inductor currents of over 2000 amps could be attained. The 800 μf capacitor in the experimental circuitry can charge the IND-1 storage inductor in about 2.3 milliseconds.



When peak current is flowing through the inductor, the crowbar ignitron is fired which creates a low impedance path, thus removing the capacitor from the circuit.

The circuit is then described schematically by



where at $t = 0$ when the crowbaring has been accomplished

$$I_i = I_s = I_0$$

$$I_l = 0$$
(21)

This is still somewhat idealized in that the interrupter switch is assumed to have negligibly small resistance.

After some "dwell time" τ_D , the interruption process begins. At this point the currents in the various parts of the circuit are

$$I_i = I_s = I_D$$

$$I_l = 0$$
(22)

After a further time interval τ_o (opening time \equiv time of arc duration)

$$\begin{aligned} I_l &= I_s = I_1 \\ I_i &= 0 \end{aligned} \tag{23}$$

the interrupter is fully open.

The energy dissipated in the resistance R_s during the dwell time is

$$\int_0^{\tau_D} R_s I_s^2 dt = \frac{1}{2} L_s I_0^2 - \frac{1}{2} L_s I_D^2 \tag{24}$$

since R_s , the inherent resistance of the inductance, is the only dissipative element in the circuit in this time interval.

The amounts of energy dissipated in the interrupter, load, and R_s during the "opening time" ($\tau_D \leq t \leq \tau_D + \tau_o = \tau$) are given by

$$E_i = \int_{\tau_D}^{\tau} V_l I_i dt \tag{25}$$

$$E_l = \int_{\tau_D}^{\tau} V_l I_l dt \tag{26}$$

and

$$E_s = \int_{\tau_D}^{\tau} R_s I_s^2 dt \tag{27}$$

Now, it is known that the summation of the energies expressed must be equal to the total energy loss of the inductor so that

$$\int_0^{\tau_D} I_s^2 R_s dt + \int_{\tau_D}^{\tau} I_s^2 R_s dt + \int_{\tau_D}^{\tau} V_L I_L dt + \int_{\tau_D}^{\tau} V_L I_i dt = \frac{1}{2} L_s I_0^2 - \frac{1}{2} L_s I_1^2 \quad (28)$$

which can be alternatively expressed as

$$\int_0^{\tau} I_s^2 R_s dt + \int_{\tau_D}^{\tau} V_L I_s dt = \frac{1}{2} L_s I_0^2 - \frac{1}{2} L_s I_1^2 \quad (29)$$

By proceeding here as in the case of the ideal circuit, we can show that

$$\frac{1}{2} L_s I_0^2 - \frac{1}{2} L_s I_1^2 < (I_0^2 R_s + I_D I_0 R_L) \tau \quad (30)$$

Again, if α is the efficiency of transfer during the interval τ , then

$$\alpha = \int_{\tau_D}^{\tau} V_L I_L dt \left[\int_{\tau_D}^{\tau} V_L I_L dt + \int_{\tau_D}^{\tau} V_L I_i dt + \int_0^{\tau} I_s^2 R_s dt \right]^{-1} \quad (31)$$

and $(1 - \alpha)$ can be expressed as

$$(1 - \alpha) \left(\frac{1}{2} L_s I_0^2 - \frac{1}{2} L_s I_1^2 \right) = \int_0^{\tau} I_s^2 R_s dt + \int_0^{\tau} V_L I_i dt \quad (32)$$

In a similar manner the total switching efficiency is

$$\epsilon = \left[\frac{1}{2} L_s I_0^2 - \int_0^{\tau} I_s^2 R_s dt - \int_{\tau_D}^{\tau} V_L I_i dt - \int_{\tau_D}^{\tau} I_s^2 R_s dt \right] \left(\frac{1}{2} L_s I_0^2 \right)^{-1} \quad (33)$$

and since the resistances R_ℓ and R_s are in series, the amount of energy that is dissipated in R_s from time τ until the current ceases is given as

$$\int_{\tau}^{\infty} I_s^2 R_s dt = \frac{1}{2} L_s I_1^2 \left[R_s / (R_\ell + R_s) \right] \quad (34)$$

showing that the fraction $R_s / (R_\ell + R_s)$ of the inductive energy at $t = \tau$ will be dissipated in the inductance.

Combining Eqs. (32), (33), and (34), we have for the efficiency

$$\epsilon = \left[E_0 - \left(\frac{1}{2} L_s I_0^2 - \frac{1}{2} L_s I_1^2 \right) (1 - \alpha) - \frac{1}{2} L_s I_1^2 (R_s / [R_\ell + R_s]) \right] E_0^{-1} \quad (35)$$

or

$$\epsilon = 1 - \frac{\left(\frac{1}{2} L_s I_0^2 - \frac{1}{2} L_s I_1^2 \right) (1 - \alpha) + \frac{1}{2} L_s I_1^2 (R_s / [R_\ell + R_s])}{\frac{1}{2} L_s I_0^2} \quad (36)$$

and with the inequality shown in Eq. (30)

$$\epsilon > 1 - \frac{(1 - \alpha)(I_1 I_D R_\ell + I_0^2 R_s) \tau + \frac{1}{2} L_s I_1^2 (R_s / [R_\ell + R_s])}{\frac{1}{2} L_s I_0^2} \quad (37)$$

Now if

$$(1 - \alpha) > \frac{(I_1 I_D R_\ell + I_0^2 R_s)(1 - \alpha) \tau + \frac{1}{2} L_s I_1^2 (R_s / [R_\ell + R_s])}{\frac{1}{2} L_s I_0^2} \quad (38)$$

then by direct substitution $\epsilon > \alpha$. Isolating τ we have

$$\tau < \frac{(1 - \alpha) \frac{1}{2} L_S I_0^2 - \frac{1}{2} L_S I_1^2 (R_S / [R_\ell + R_S])}{(1 - \alpha) (I_1 I_D R_\ell + I_0^2 R_S)} \quad (39)$$

This inequality is still valid if we substitute I_0 for I_1 and I_D since both the latter are smaller than I_0 .

$$\tau < \frac{(1 - \alpha) - R_S / (R_\ell + R_S)}{2(1 - \alpha)} L_S / (R_\ell + R_S) \quad (40)$$

makes the value of ϵ larger than α .

Lastly, we can express the ratio of R_S to $(R_\ell + R_S)$ as

$$R_S / (R_\ell + R_S) = (R_\ell + R_S - R_\ell) / (R_\ell + R_S) = 1 - R_\ell / (R_\ell + R_S) \quad (41)$$

and rewriting Eq. (40)

$$\tau < \frac{[(1 - \alpha) - (1 - R_\ell / [R_\ell + R_S])] L_S / (R_\ell + R_S)}{2(1 - \alpha)} \quad (42)$$

$$\tau < \frac{[R_\ell / (R_\ell + R_S) - \alpha] L_S / (R_\ell + R_S)}{2(1 - \alpha)} \quad (43)$$

It is easy to see here that

$$\alpha > R_\ell / (R_\ell + R_S) \quad (44)$$

does not correspond to a real situation since it implies that τ is negative.

When a is maximum

$$\epsilon = a_{\max} = R_l / (R_l + R_s) \quad (45)$$

and the transfer efficiency is the best possible in the realistic circuit. We refer to this as a perfect transfer.

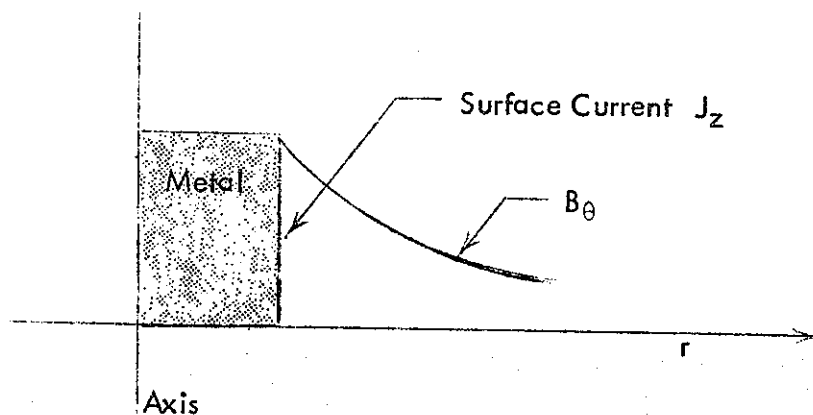
B) STABILITY OF A LIQUID METAL COLUMN

During the course of this investigation we have examined the feasibility of using streams of liquid metals as interrupter elements. Two basic configurations appeared of practical interest and a number of interruption schemes have been studied conceptually and in experiments. The first geometry is columnar and the second is tubular; in each case the problem of primary importance is the stability of the metallic conductor during current passage and its susceptibility to external perturbing forces. We first consider the stability of a jet of liquid metal. This problem can be treated satisfactorily with the hydromagnetic theory, especially if one neglects viscosity and resistivity. The neglect of viscosity does not change the stability conditions, but does reduce the growth rates of instabilities when the stability conditions are violated. The presence of viscosity just increases the effective mass density somewhat. The neglect of resistivity changes the stability conditions. In the case of the solid column of liquid metal, this is relatively unimportant, however, since the situation is always unstable anyway, even on the

perfect-conductivity model, and since the additional instabilities introduced by allowing for finite resistivity are relatively slow-growing.

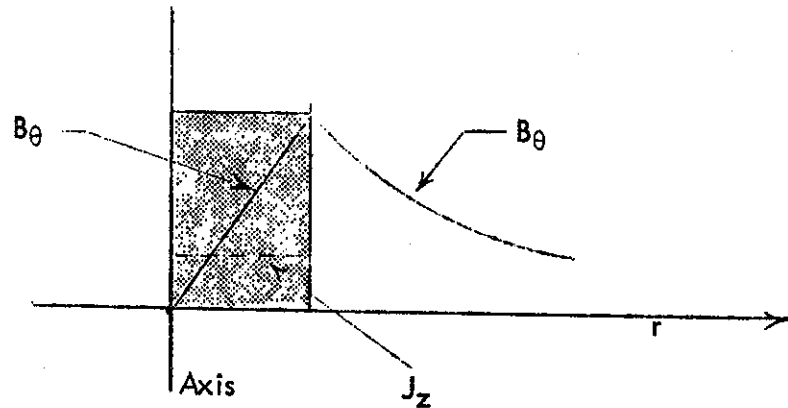
The surface tension can have an appreciable effect on short-wave modes, but has little effect on strongly unstable gross modes of the column. Fortunately, one can treat the liquid metal as being incompressible to a very good approximation. This assumption has no effect on the stability conditions, except for the special case of axisymmetric modes, but it greatly simplifies the problem of obtaining growth rates.

We will thus consider simply the idealized incompressible hydromagnetic model, without dissipative effects on surface tension. This stability problem has often been treated for a current flowing in a thin layer on the surface of the column:



Model 1

This simple Model 1 is easy to handle, but differs significantly from the actual case, where the axial current density J_z is distributed uniformly over the cross-section of the column:



Model 2

There is a substantial difference both in stability conditions and growth-rates. For present purposes, one should treat the more realistic Model 2 in order to get exact results--or simply content oneself with the rough estimates obtained from

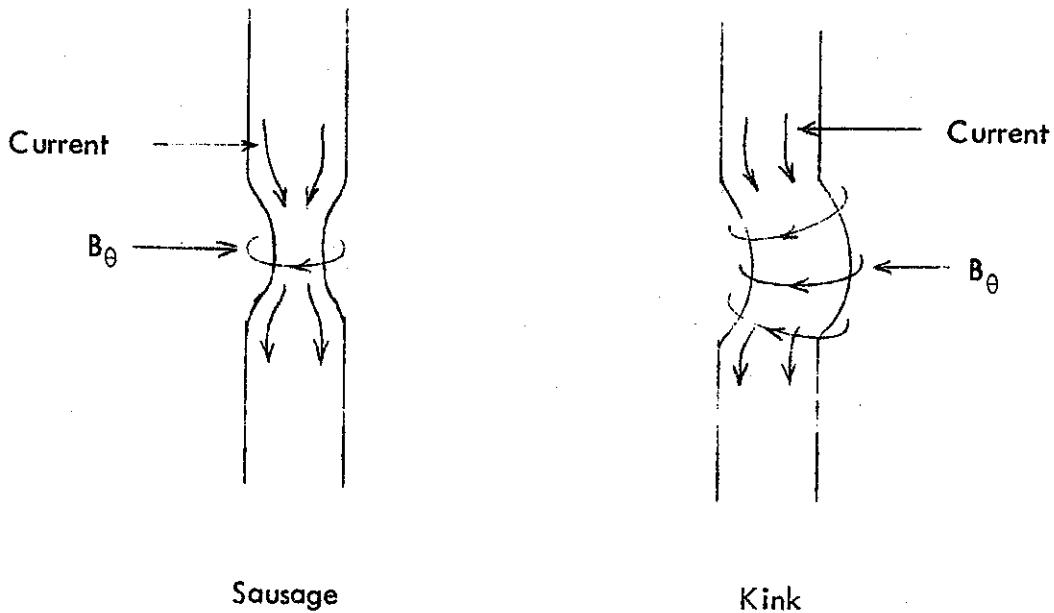
$$\omega = v_a / \lambda \quad (46)$$

where ω is the growth rate, v_a is the Alfvén velocity

$$v_a = B / \sqrt{4\pi\rho} \quad (47)$$

and λ is the wave-length. Here B is the magnetic field strength and ρ is the mass density.

The two types of instability that are most prominent in the columnar configuration are the "sausage" mode and the "kink" mode:



In terms of the usual Fourier-analysis approach, we represent the instability perturbations in the form

$$\bar{v}[r, \theta, z] = \bar{v}_0[r] \exp\{i(kz + m\theta)\} \quad (48)$$

where $m = 0$ for the sausage and $m = 1$ for the kink mode. The most dangerous wavelength $\lambda = 2\pi/k$ for the sausage mode is usually comparable to the diameter of the column. For the kink mode, the most dangerous wavelength may be slightly longer.

Turning now to exact analysis, we can immediately put down some general stability conditions due to Kadomtsev.¹

For the $m = 0$ mode, a necessary and sufficient stability condition is

$$(r/B_{\theta}) (dB_{\theta}/dr) < 1 \quad (49)$$

(where we have used the incompressibility condition to simplify Kadomtsev's result). We see immediately that the Model 1 configuration is highly unstable since dB_{θ}/dr is very large at the surface. On the other hand, the Model 2 configuration has $B_{\theta} \rightarrow r$, and thus is marginally stable if J_z is really uniform.

A necessary condition for $m = 1$ stability is

$$(r/B_{\theta}) (dB_{\theta}/dr) < -1 \quad (50)$$

This is always violated by the columnar model, and so there is always the danger of break-up by kinks.

As soon as a kink starts (or if there is any other type of time-variation also in J_z) the sausage mode can also set in and finish off the interruption of the current.

C) STABILITY OF A TUBULAR LIQUID METAL FLOW

A liquid metal stream has great advantages as an interrupter element. It renews itself rapidly, at a rate that can be controlled by the flow velocity and length, and it has neither heat removal nor surface-deterioration problems. Thus, it lends itself to operation at fairly high repetition rates and for extended times.

The main disadvantage of the simple columnar liquid metal stream is that it can carry only limited currents, since it is so extremely unstable against "nipping off". For liquid metal columns of practical dimensions, this limits the operation to something like a few thousand amperes. In applications requiring currents of tens of thousands or hundreds of thousands of amperes, it is desirable to look for another configuration, which can carry such currents in stable equilibrium for extended times prior to the desired interruption.

Fortunately, there exists one extremely stable configuration which has the desired properties. By using a tubular flow of liquid metal, and placing the current-return conductor coaxially on the inside rather than on the outside (Fig. 1), we can achieve magnetohydrodynamic stability against all modes in the limit of perfect conductivity. This leaves only slowly growing finite resistivity modes, or can even give perfect stability. The basic idea is easily recognized in Fig. 2. If an ordinary current-carrying column is perturbed, the magnetic field is strongest at those points where the column is already too narrow (since $B_{\theta} \sim I/r$) and therefore the perturbation grows. If the current-carrying tube is perturbed, the magnetic pressure drops at those points where the tube is bulged out and increases at those points where it protrudes in. Therefore, the situation is expected to be stable.

This type of configuration was invented by H. P. Furth in 1958 in connection with thermonuclear plasma devices. Its effectiveness in giving stable plasma currents was

demonstrated by O. A. Anderson, H. P. Furth, et al.² Its effectiveness with liquid metals was demonstrated in plasma simulation experiments by K. Aitken, R. Bickerton, et al.³

In typical operation for interruption of a large current, one begins with a tubular liquid metal stream on the outside of an insulating tube (Fig. 3). Where the dc current is passed through the liquid metal, a magnetic field B_θ appears between the liquid metal tube and the central conductor. The tube then expands away from the insulator, and the outward magnetic pressure current is balanced by an external gas pressure. For currents in the range 10 - 100 ka, the typical magnetic pressures will be of the order of a few atmospheres, which is easily matched with external gas pressure. An equilibrium is thus readily achieved at a predetermined radius. (Since the magnetic pressure $B_\theta^2/8\pi$ drops with the square of the tube radius while the gas pressure is constant, the liquid metal tube will easily adjust itself to equilibrium.)

The real problem is how to upset this stable situation so as to bring about current interruption. As already mentioned, the only possible instabilities are those associated with finite resistivity. These typically involve filamentation along current flow lines, rather than fluting along magnetic field lines, which is typical of the perfect conductivity case.⁴

We must therefore seek to induce such filamentation in the axial direction. One suitable scheme for this purpose is shown in Fig. 4. The auxiliary circuit

tends to create an axial tear in the liquid metal tube by passing a reverse current and thus weakening the current in the tube in the region near the auxiliary circuit. The liquid metal then is strongly attracted toward the other side of the central conductor where it now forms a column of liquid metal. The column is highly unstable against nipping off, and the current is interrupted. The use of the external gas for pressure equilibrium has the extra merit of causing the liquid metal tube to blow out when the initial tear appears (the outward magnetic pressure then being unbalanced). It also helps to quench the arc between liquid metal segments after nipping off occurs.

The tubular liquid metal interrupter thus has the great advantage of allowing an explosive situation to be built up stably at high magnetic and gas pressures, which is then triggered off to give a powerful current interruption. In this sense, it represents a radical improvement over other interruption methods where the interruption energy is either small, and relatively ineffective, or else imposes an inconvenient auxiliary energy requirement. Coupled with the basic advantages of the liquid metal stream method, which we have already mentioned, the tubular interrupter should have a uniquely effective and practical application in the area of high currents and high repetition rates.

D) COMPARISON OF LIQUID METALS FOR FLUID-TO-FLUID INTERRUPTION

The properties of several different metals have been examined to determine the materials most suitable for use in the fluid-to-fluid interrupter switches. The first and most restrictive condition in this respect is that the metallic conductor must be a liquid at, or near, room temperature. Thus, all metals with melting points above 100°C have been ruled out with the exception of lithium (Li) whose exceptionally low density makes it a possible candidate in spite of its 179°C melting point. Other materials that could prove suitable for this purpose include mercury (Hg), potassium (K), sodium (Na), sodium-potassium (NaK) alloys, and gallium (Ga).

Of the various physical properties, the two most important ones are density and electrical resistivity. A low density metallic fluid is better suited for this type of interruption than a higher density liquid because less force (energy) is required to separate a filament or column of the fluid. Densities of the various metals as functions of temperature^{5, 6, 7} are shown in Figs. 5 through 11. The densities of two different sodium-potassium alloys (56 Na-44K and 22 Na-78 K) are shown in Figs. 8 and 9. The numbers here (56 Na) refer to the percentage composition by weight. In order of increasing density at their melting point the materials are Li, K, 22 Na-78 K, 56 Na-44 K, Na, Ga, and Hg.

Low electrical resistivity is also a desirable feature for metals in this application for two reasons. Since high currents are passed through the metal, I^2R

losses are smaller, and a high conductivity fluid is easier to manipulate with a pulsed magnetic field due to its smaller skin depth. Figures 12 through 17 show the electrical resistivities of these metals (gallium excepted) as functions of their temperature. Data available on gallium is insufficient to graph this functional relationship, however, the electrical resistivity at 46°C is given as 28.4 micro-ohm cm.⁶ These materials, listed in order of increasing resistivity are Na, K, Li, Ga, the two NaK alloys, and Hg.

Factors other than the physical properties are also of importance in determining the applicability of these metals to fluid-to-fluid interrupters. Material compatibility of the liquid metal with its surroundings is a problem which affects all alkali metals. The present experimental work with sodium (one of the less reactive alkali metals) bears this out. Compounds of sodium and nitrogen were formed during the interruption process and in one instance an exothermic reaction between sodium and teflon was observed. Ceramics appear to be the best possibility in terms of compatible materials. However, data on the behavior of ceramics exposed to a high temperature alkali metal plasma are not available at present. When material compatibility problems are solved, lithium, sodium, or the NaK alloys look very promising indeed for the fast interruption of large currents.

References:

- ¹ B. B. Kadomtsev, *Soviet J. Exp. Theor. Phys.* 37, 780 (1959).
- ² O. A. Anderson, H. P. Furth, J. M. Stone, R. E. Wright, *Phys. of Fluids* 1, 489 (1958).
- ³ K. Aitken, R. Bickerton, R. Hardcastle, J. Jukes, P. Reynolds, I. Spalding, *Nuclear Fusion* 2, 987 (1962).
- ⁴ H. P. Furth, J. Killeen, *Phys. of Fluids* 6, 459 (1963).
- ⁵ The Handbook of Chemistry and Physics, 45th Edition (The Chemical Rubber Co., 1964).
- ⁶ Clifford A. Hampel, Rare Metals Handbook, 2nd Edition (Reinhold Publishing Co., 1961).
- ⁷ National Research Council of the U. S., International Critical Tables of Numerical Data, Physics, Chemistry, and Technology, Vols. I-VII (McGraw-Hill Book Company, Inc., New York).

II) EXPERIMENTAL PROGRAM

A) INTRODUCTION

Previous contractual studies¹ have resulted in the design and development of several types of interruption devices for use in the switching of inductively stored energy. In some cases, high energetic efficiencies were attained in the single-shot mode of operation, but the use of solid material as one or both of the contacts was a drawback common to all of these switches. During the interruption process very high current densities are reached at the last point of contact between the electrodes. The resultant localized energy dissipation is sufficient to vaporize portions of the electrode material. Scarring and cratering of the electrodes in this manner make subsequent interruptions considerably less efficient; consequently, operation at finite repetition rate with these devices has not been entirely practical.

The design philosophy of the interrupter switches used in the present studies has therefore been to make the contacts on both sides of the interruption point of a metallic fluid. The electrodes are then self-healing and the erosion problem is avoided.

B) SINGLE-CELL MULTI-SHOT INTERRUPTER (MSI-3)

1) Design Considerations

The design of the MSI-3 interrupter switch was motivated by the need of a switching device whose electrodes would not be damaged by repetitive interruption operation. In this regard, electrodes of any solid material were unsuitable because of the aforementioned erosion which results in lower efficiencies.

The MSI-3 configuration is shown in Fig. 18; it consists essentially of two connected metallic pools embedded in an insulating material. The pools are connected across a septum of the same insulating material by a thin liquid metal filament. A high-field pulsed magnet² is situated above the septum. When energized, the magnet causes the metallic surface to be depressed, thereby exposing the septum and preventing electrical contact between the pools of liquid metal. The metallic liquid presents a self-healing contact surface even at the very high temperatures that are produced during the last point of contact.

To obtain a high voltage hold-off between the metallic pools during the interruption process, the switch body was constructed from a 1/4" thick stainless steel cylinder to accommodate a high pressure gas atmosphere above the metallic surface. High pressure gas has the effects of making the arc more resistive and of shortening the arc duration.

Design of the MSI-3 allows for the use of pressures greater than 600 psi within the switching chamber. Comparisons between the results of atmospheric pressure interruptions and higher pressure experiments verify the expected advantage of operating in the high pressure regime.

The metallic pools are located in a machined teflon insert which fits into the lower portion of the switch body. Teflon was chosen as the insulating material because of its chemical inertness and machinability. Electrical connections to the pools are made through the bottom of the switching chamber via copper electrodes. These electrodes are hollow to accommodate heating elements for experiments with liquid sodium.

The pulsed magnet is connected to the upper half of the switch body and its electrical connections enter from the top, as shown in Fig. 18. Bolting the two halves of the switch body together forms a pressure-tight seal.

The MSI-3 configuration constitutes a significant contribution to the understanding of fluid-to-fluid interruption devices and it has become a valuable stepping-stone towards the development of more advanced models.

2) Operational Results with Mercury

a) Self-Interruption Mode of Operation

The mechanism of self-interruption has been quite useful in determining the characteristic properties of the various interrupter switches.

With mercury as the interrupting medium, the MSI-3 has undergone two

testing sequences in the self-interruption mode of operation. One series was performed with a constant pressure (14.5 psi of nitrogen) in the switching chamber at various peak inductor currents. The other testing sequence was done at a constant peak inductor current and a variable pressure (14.5 psi to 500 psi).

The circuitry used in these experiments is represented schematically in Fig. 19. The "zero time" ignitron discharges an 800 μ f capacitor bank into the IND-1 inductive storage unit ($L = 2.4$ mh). When the current in the inductor has reached peak, the crowbar ignitron effectively shorts out the capacitor resulting in a slow decay of the current due to the inherent circuit resistance.

During testing of a particular series, the cross-sectional area of the current-carrying fluid filament was kept as constant as possible. However, maintaining identical cross-sections from series to series was not entirely feasible in that switch disassembly was sometimes necessary and new metallic fluid was added. Consequently, whereas comparison between individual efficiencies or voltages in two different testing sequences is not wholly valid, comparison of the trends shown in the various sequences is very indicative.

Table I shows the data obtained with a .43 ohm load and various peak inductor currents. Within the switching chamber nitrogen gas was maintained

TABLE I
MSI-3

SELF-INTERRUPTION (MERCURY) ATMOSPHERIC PRESSURE NITROGEN

Bank Voltage (kv)	Bank Energy (joules)	Max. Inductor Current (amps)	Dwell Time τ_D (msec)	Arc Duration τ_0 (msec)	Energy* of Perfect Transfer (joules)	Max. Voltage in Perfect Transfer	Energy Transferred to Load (joules)	% of Total Energy	% of Perfect Transfer	Max. Voltage Across Load
1.0	400	580	11.5	3.0	324	250	50.9	12.7	15.7	75.7
1.5	900	870	6.4	10	729	372	83	9.2	11.3	64.3
2.0	1600	1150	4.7	13	1300	500	131	8.2	10.1	85.7

*with .43Ω load

TABLE II

MSI-3 SELF-INTERRUPTION (MERCURY) PRESSURIZED NITROGEN

Pressure Inside Switch	Energy of Perfect Transfer (joules)	Energy Transferred to Load (joules)	% of Total Energy Transferred	% of Perfect Transfer	Dwell Time (msec)	Maximum Voltage Hold-off
14.5	2010	283	11.5	14	2.4	116
100	2010	605	24	30	7.5	273
200	2010	540	21.5	26.5	11	276
300	2010	840	33.5	41	4.5	281
400	2010	880	35	43	5.0	288

Bank Energy 2500 joules; Maximum Inductor Current 1450 amps; Load .43 Ω

at a constant pressure of 14.5 psi. As seen in Table I, even though the amounts of energy transferred to the load increase with increasing inductor currents, the transfer efficiencies are at the same time decreasing.

Figures 20 through 24 show the data from Table I in graphical form and also compare the results with those obtained from a similar series taken with sodium.

Table II contains the data obtained in the self-interruption mode with mercury at constant peak inductor current and at elevated pressures.

Figure 25 is a plot of dwell time versus pressure for this series of shots. (The dwell time is defined here as the time interval between peak current and the beginning of the interruption process.) The two highest pressure shots and the first three are to be grouped separately as different mercury levels were used. Within the groups, however, there is a trend for increased pressure to produce an increased dwell time. Figure 26 shows the percent of energy transferred to the load versus pressure since the inductor energy for this series was constant.

b) Powered-Interruption Mode

In the powered-interruption mode of operation, there are three forces that can contribute towards breaking the liquid metal filament connecting the two metallic pools in the MSI-3 configuration. The first is the tendency of the filament to self-pinch due to the effect of the current carried. The

second is the $\vec{I} \times \vec{B}$ force on the filament from interactions with the driver coil and the third is the magnetic pressure exerted on the metallic surface by the rapidly varying \vec{B} field of the driver coil.

In the experimental sequence with mercury, the second force is negligibly small since the driver coil was positioned such that the pulsed field was parallel to the current. Since most of the field lines from the driver coil have little effect on the metallic surface (see Fig. 18), energetic coupling between the fluid and coil is somewhat inefficient. To reduce the tendency towards self-interruptions, a filament with a larger current carrying area was used (the fluid level in the powered-interruption mode was higher). Thus, the driver coil was the main contributor to the interruptions observed in this series of experiments.

An outline of the data compiled during these experiments is shown in Table III. As seen in Figs. 27 and 28, interruption efficiencies seem to be relatively independent of pressure. The marked contrast between these results and the results of the self-interruption mode (cf. Figs. 20, 23, 24, 26) are due in part to the higher level of fluid across the septum necessary in this experimental series. Figure 29 compares the hold-off voltages with the maximum hold-off voltage that would occur in a perfect transfer.

TABLE III

POWER INTERRUPTION OF MERCURY

Bank Voltage (kv)	Bank Energy (joules)	Max. Inductor Current (amps)	Energy* of Perfect Transfer (joules)	Pressure (psi)	Energy Transferred to Load	% of Total Transfer	% of Perfect Transfer	Max. Voltage in a Perfect Transfer	Max. Voltage across the Load
1.5	900	870	630	14.5	162	18	26	129	73
1.5	900	870	630	100	168	18.7	27	129	90
1.5	900	870	630	300	104	11.5	16.5	129	79
1.5	900	870	630	500	156	17.3	25	129	93
2.0	1600	1150	1120	14.5	250	15.6	22.3	143	82
2.0	1600	1150	1120	100	252	15.7	22.5	143	112
2.0	1600	1150	1120	300	281	17.5	25	143	115
2.0	1600	1150	1120	500	251	15.7	22.4	143	115

* with .23Ω load

3) Operational Results with Sodium

a) Self-Interruption

Testing of the MSI-3 liquid metal interrupter switch was performed using both mercury and liquid sodium as interrupting media. As with the self-interruption experiments conducted with mercury, sodium self-interruption operations have included two distinct sequences. Initial operations were confined to atmospheric pressure dry nitrogen above the interrupting surface. A second experimental series was performed at elevated pressures and constant bank voltage.

Liquefaction of the sodium was attained by the use of heaters embedded in the electrodes, as shown in Fig. 30.

Data obtained at atmospheric pressure and various peak inductor currents are shown in Table IV. The results outline dramatically the superiority of sodium as a switching medium. Not only are the "percent of energy transferred" values higher, but the slope of the "percent of perfect transfer" versus "inductor current" is positive as opposed to the negative slope with mercury (see Fig. 20). Figure 21 shows the dwell time (the time between peak inductor current and the opening of the switch) for both metals as a function of the peak current in the inductor.

As expected, the pinching effect of self-interruption is hastened with larger currents and the lighter medium. Shown in Fig. 22 are data relating

TABLE IV

MSI-3

SELF-INTERRUPTION (SODIUM) ATMOSPHERIC PRESSURE NITROGEN

Bank Voltage (kv)	Bank Energy (joules)	Peak Inductor Current (amps)	Dwell Time τ_D (msec)	Arc Duration τ_0 (msec)	Energy* of Perfect Transfer (joules)	Maximum Voltage in Perfect Transfer	Energy Transferred	% of Total Energy	% of Perfect Transfer	Max. Voltage Across Load
1.0	400	580	8.5	0.3	324	250	78	19.4	24	92.9
1.5	900	870	4.7	1.7	729	372	325	36.2	45	183
2.0	1600	1150	2.3	4.3	1300	500	1230	77.0	95	346

*with .43 Ω load

the arc duration to the inductor current. Again, sodium is superior. Because of its lower density and higher conductivity, it apparently moves apart farther, lengthens the arc path and hence quenches the arc faster. Figures 23 and 24 are the percent of total energy transferred and the percent of perfect transfer as functions of the total inductor energy, respectively.

Nitrogen atmosphere high-pressure testing of the liquid sodium MSI-3 interrupter switch was also done for the self-interruption mode of operation. The formation of a brownish-black compound (possibly sodium azide)³ when interrupting in the nitrogen atmosphere led to the use of argon in the interrupting chamber. Data compiled in the nitrogen and argon series are exhibited as Tables V and VI, respectively.

It is the intent of the self-interruption testing of the MSI-3 to illustrate trends in the percentage energy transfer with a constant height of fluid metal in the interrupting channel. However, even in a particular series, identical fluid heights from shot-to-shot are impossible. Switching efficiency in a particular shot depends somewhat on the previous shots. For this reason, anomalous values, such as the high percent of perfect value in Table VI (1600 joule bank energy and 500 psi), occur occasionally. This shot is probably the result of the switch resetting in such a way that only a very small filament of liquid sodium was connecting the two pools.

TABLE V
 SELF-INTERRUPTION (LIQUID SODIUM) PRESSURIZED NITROGEN

Pressure	Bank Energy	Max. Inductor Current	Energy* of Perfect Transfer	Energy Transferred to Load	% of Total Energy	% of Perfect Transfer	Maximum Voltage Across Load	Maximum Voltage in a Perfect Transfer
100	1.0	580	280	208	52	74	108	133
	1.5	870	630	344	38	55	144	200
	2.0	1150	1120	883	55	79	191	265
300	1.0	580	280	224	56	80	118	133
	1.5	870	630	480	53	76	161	200
	2.0	1150	1120	904	57	81	225	265
500	1.0	580	280	196	49	70	104	133
	1.5	870	630	495	55	79	144	200
	2.0	1150	1120	572	47	67	209	265

* with .23Ω load

TABLE VI

SELF-INTERRUPTION (LIQUID SODIUM) PRESSURIZED ARGON

Pressure	Bank Energy	Max. Inductor Current	Energy* of Perfect Transfer	Energy Transferred to Load	% of Total Energy	% of Perfect Transfer	Maximum Voltage Across Load	Maximum Voltage in a	
								Perfect	Transfer
100	1.0	580	280	278	70	88	125	133	
	1.5	870	630	481	53	76	129	200	
	2.0	1150	1120	624	39	56	143	265	
300	1.0	580	280	136	34	48	97	133	
	1.5	870	630	278	31	44	131	200	
	2.0	1150	1120	309	19	28	157	265	
500	1.0	580	280	96	24	34	80	133	
	1.5	870	630	235	26	37	106	200	
	2.0	1150	1120	717	45	64	209	265	

* with .23 Ω load

Figures 31 and 32 are graphs of percent of perfect transfer versus pressure for nitrogen and argon, respectively. With the exception of the one rather low value in Fig. 31, there is no particular relationship of pressure on the percent of perfect transfer curve. Figure 32, however, shows a definite tendency in argon for increasing pressure to produce decreasing switching efficiency. From Figs. 27 and 28, it was seen that with mercury as the interrupting medium, significant increases in switching efficiencies were effected by increasing the pressure. It appears, therefore, that the high pressure gases inhibit the motion of sodium to a greater degree than that of mercury.

With sodium, then, in the nitrogen atmosphere, voltage stand-off capabilities due to the high pressure are offset by a shorter arcing path. Argon due to its lower ionization voltage reverses the trend of higher efficiencies with higher pressures.

Figures 33 and 34 show the percent of perfect transfer versus maximum inductor current for different pressures of nitrogen and argon.

b) Powered-Interruption Mode

Experimentation was performed with the MSI-3 interrupter switch with liquid sodium as the interrupting medium and in the driven mode of operation. The driver coil was again mounted so that the \bar{B} -field was parallel to the filament current. This coil ($L \sim 8 \mu\text{h}$) was energized from a $30 \mu\text{f}$ capacitor

bank with voltage capabilities of 8 kv. Field intensity measurements of this configuration with an aluminum plate positioned so as to simulate the presence of the liquid metal indicated a 3 kgauss/kv field at the interruption point. The field rises from zero to the above value in about 20 μ sec.

Results from the powered interruption mode with sodium are shown in Tables VII and VIII. Only a slight increase in efficiency is noted as the pressure is increased. A comparison with the values in Table III (page 31), however, shows sodium to be 2.5 times as efficient as mercury in the driven mode.

C) TRIPLE-CELL MULTI-SHOT INTERRUPTER (MSI-4)

1) Design Considerations

Because of the desire to attain a higher voltage hold-off than seemed possible with the MSI-3 configuration, a switch was designed which incorporated three points of interruption in series, thus increasing the impedance of the switch during operation by a factor of about three. The interruption chamber was again machined of teflon and was designed to fit in the MSI-3 switch body.

Two teflon inserts were used; these are labeled MSI-4P and MSI-4T to indicate that the \bar{B} field of the driver coil and the current density \bar{i} are parallel to each other (-4P) or perpendicular (transverse, -4T). These inserts are illustrated diagrammatically in Figs. 35 and 36.

TABLE VII

POWER INTERRUPTION OF SODIUM AT ATMOSPHERIC PRESSURE (NITROGEN)

Bank Voltage (kv)	Bank Energy (joules)	Max. Inductor Current (amps)	Energy of Perfect Transfer (joules)	Energy Transferred to Load	% of Total Transfer	% of Perfect Transfer
1	400	580	280	117	29.3	42
1.5	900	870	630	254	28.3	40.5

TABLE VIII

PRESSURIZED POWER INTERRUPTION OF SODIUM (NITROGEN)

Pressure (psi)	Bank Voltage (kv)	Bank Energy (joules)	Max. Inductor Current (amps)	Energy of Perfect Transfer (joules)	Energy Transferred to Load	% of Total Transfer	% of Perfect Transfer
100	1.5	900	870	630	292	33	47.2
300	1.5	900	870	630	320	35.5	50.7
500	1.5	900	870	630	322	35.7	51

Certain modifications also were made in the base of the switch body to accommodate electrodes and heater elements for all four metallic pools. Also, a different driver coil was designed and installed in the upper section of the switch body. A cross-sectional model of the MSI-4T is shown in Fig. 37.

Only the insert is changed in the MSI-4P.

One of the more difficult aspects of working with this switch is that of keeping the cross-sections of the three metallic filaments as nearly equal as possible so that interruption occurs at the same time.

In both these configurations the same driver coil is used. The coil is similar to those used in the SSI series of switches⁴ (a pancake coil wound out of copper strip). The coil is positioned parallel to the interrupting fluid and just above it. A much better magnetic coupling than that of the MSI-3 was achieved because of the greater compression of the magnetic field flux in this configuration.

2) Results with the MSI-4P

A complete set of data was taken with the MSI-4P with mercury as the interrupting medium. The self-interrupting mode of operation with the MSI-4 type switch is not particularly applicable in that interruption of one of the filaments would prevent the others from breaking, thus negating the use of three simultaneous interruption points.

Table IX presents the significant results obtained with the MSI-4P. As in previous switches, it is noted that efficiency increases with pressure. In this case,

TABLE IX
MSI-4P
DRIVEN-INTERRUPTION (MERCURY) PRESSURIZED NITROGEN

Pressure (psi)	Bank Voltage (kv)	Bank Energy (joules)	Max. Inductor Current (amps)	Energy* of Perfect Transfer (joules)	Energy Transfer to Load	% of Total Energy	% of Perfect Transfer	Max. Voltage in Perfect Transfer	Max. Voltage Across Load	% of Maximum Voltage Attained
14.5	1.0	400	580	323	212	53	66	244	127	52
	1.5	900	870	727	486	54	67	365	217	59
	2.0	1600	1150	1292	531	33	41	483	186	39
100	1.0	400	580	323	222	56	69	244	161	66
	1.5	900	870	727	497	55	68	365	206	56
	2.0	1600	1150	1292	747	47	58	483	234	48
300	1.0	400	580	323	258	65	80	244	178	73
	1.5	900	870	727	544	60	75	365	208	57
	2.0	1600	1150	1292	1143	71	88	483	366	76
500	1.0	400	580	323	228	57	71	244	161	66
	1.5	900	870	727	535	59	74	365	217	59
	2.0	1600	1150	1292	1114	70	86	483	366	76

*with .42Ω load

dry nitrogen is used as the pressurizing agent. Best hold-off voltages are observed to be approximately 75% of the maximum attainable, with 366 volts being the highest value achieved with a .42 ohm load. Also observed are energy transfers of approximately 90% of perfect into this particular load. It should be noted that this is the first instance of efficient energy transfer beyond 1 kJ.

The graph, Fig. 38, shows the percent of perfect transfer versus pressure from the data presented in Table IX.

Higher resistance loads have been considered for use with the MSI-4. From the data obtained with mercury, this switch seems to allow for the possibility of transfer efficiency in excess of 70 - 80% into loads of 1 to 2 ohms, or perhaps even higher loads.

Sodium testing was initiated in the MSI-4 while still retaining the $\bar{I} \parallel \bar{B}$ teflon insert. When interruption was attempted, a self-sustaining chemical reaction was started in the interruption chamber of this switch. Pressure produced by this reaction rapidly increased to such an extent that the top section of the switch was blown off. Pressure has been estimated to be in excess of 5000 psi. The reaction, believed to be the result of sodium combining with fluorine in the teflon, had not been observed in prior work with the MSI-3 due to the low surface-to-volume ratio of the teflon in that configuration. In the MSI-4 the teflon separators apparently allowed a sufficient contact surface to maintain the reaction triggered by the arc. Mention appears in the literature⁵ of the use of alkali metal dispersions

for extracting fluorine from teflon, but no indication is given of the possibility of developing an exothermic reaction as encountered above. At the present state of materials technology, there does not appear to be an insulating material known to be inert to a high temperature alkali plasma as formed during the interruption process. The damage to the driving coil and teflon insert made them irreparable. The switch container, however, was sufficiently sturdy so that damage to it was slight.

After building another driving coil, testing was continued with the MSI-4T (\bar{I} and \bar{B} transverse) and a mercury interrupting medium.

3) Results with the MSI-4T

Because of the chemical reaction that was produced in the sodium operation of the MSI-4P, experimentation with the MSI-4T was conducted only with mercury. Testing in this regime has included the use of argon as the pressurization agent in an attempt to reduce contamination of the mercury.

Table X shows efficiencies, voltages and other parameters calculated from a set of data taken with a 1-ohm load and using an argon atmosphere. Table XI compares results obtained at various pressures of nitrogen in the MSI-4T with a load of .42 ohm. Comparison of this data with that presented in Table VIII shows the results of the two different inserts under identical conditions.

As postulated previously, the use of a higher load increases the voltage developed across the interrupter. In a 1-ohm load circuit with 500 psi of nitrogen,

TABLE X

MSI-4T

DRIVEN-INTERRUPTION (MERCURY) PRESSURIZED ARGON

Pressure (psi)	Bank Voltage (kv)	Bank Energy (joules)	Max. Inductor Current (amps)	Energy* of Perfect Transfer (joules)	Energy Transfer to Load	% of Total Energy	% of Perfect Transfer	Max. Voltage in Perfect Transfer	Max. Voltage Across Load	% of Max. Voltage Attained
14.5	1.0	400	580	360	27.4	6.8	7.6	580	90	16
	1.5	900	870	810	45.0	5.0	5.5	870	62	7.1
	2.0	1600	1150	1440	93.1	5.8	6.5	1150	136	12
100	1.0	400	580	360	---	---	---	---	---	---
	1.5	900	870	810	51	5.6	6.3	870	93	11
	2.0	1600	1150	1440	118	7.3	8.2	1150	118	10
300	1.0	400	580	360	77.2	19.3	21.4	580	170	29
	1.5	900	870	810	202	22.4	24.9	870	200	23
	2.0	1600	1150	1440	388	24.3	26.9	1150	317	28
500	1.0	400	580	360	35.5	8.9	9.8	580	149	26
	1.5	900	870	810	160	17.7	19.7	870	214	25
	2.0	1600	1150	1440	453.3	28.3	31.5	1150	350	30

*with 1 Ω load

TABLE XI

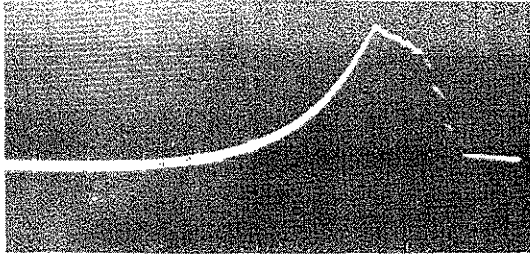
MSI-4T

DRIVEN-INTERRUPTION (MERCURY) PRESSURIZED NITROGEN

Pressure (psi)	Bank Voltage (kv)	Bank Energy (joules)	Max. Inductor Current (amps)	Energy* of Perfect Transfer (joules)	Energy Transfer to Load (joules)	% of Total Energy Transfer	% of Perfect Transfer	Max. Voltage in Perfect Transfer	Max. Voltage Across Load	% of Max. Voltage Attained
100	1.0	400	580	323	123	31	38	244	109	45
	1.5	900	870	727	218	24	30	365	148	41
	2.0	1600	1150	1292	---	---	---	483	---	---
300	1.0	400	580	323	108	27	33	244	100	41
	1.5	900	870	727	411	41	56	365	246	68
	2.0	1600	1150	1292	479	30	42	483	214	44
500	1.0	400	580	323	158	39	49	244	149	61
	1.5	900	870	727	374	41	51	365	180	49
	2.0	1600	1150	1292	713	45	62	483	206	43

*with .42 Ω load

490 volts were observed across the load. This is shown in the oscillogram below.



200 v/cm; 2 msec/cm
IND-1 charged to 2500 joules
500 psi nitrogen
1 Ω load
Driver coil energized from 30 μ f
capacitor bank @ 6 kv.

Testing of the MSI-4 interrupter switch configuration was thus concluded. The decision to discontinue testing of the MSI-4 sodium and mercury device was based on three factors: (a) the present lack of an adequate dielectric material for use with sodium in the presence of a high temperature arc; (b) the somewhat random energy transfers due to variations in the depth of the liquid metal upon resetting, and (c) the development of a prototype switch that appears to offer several advantages over previous models.

D) COLUMNAR VERTICAL FLOW INTERRUPTER (CVFI)

After limited success with the MSI-4 configuration, a new mode of operation was investigated. The new switch requires no dielectric material at the point of interruption, except perhaps pressurized gas. This switch, labeled the CVFI (columnar vertical flow interrupter) is shown in Fig.39. A liquid conductor is placed in two reservoirs, one situated above the other at height h . Electrical contacts are made with both liquid pools and connected so that the switch is electrically in parallel with the desired load. The switch is equipped with a nylon plunger valve to control the liquid flow. The liquid in the upper reservoir passes through this valve into the running tube which has a diameter of slightly over 3 mm, past the tube orifice, and into free fall. It is in the free fall region that the experimental work was conducted.

This configuration has the additional advantage of automatically resetting itself after interruption, thus showing its applicability for repetition rate operation. The "open time" of this switch is determined by the distance between the lower reservoir and the point of interruption. The configuration could also be easily converted to a "multi-interrupter" by causing the column to break simultaneously at several points.

Experimentation was first undertaken to determine the stability of the vertical column with respect to relatively high current pulses. Subsequent testing of the CVFI was aimed at demonstrating that an externally applied pulsed magnet field

could interrupt the column.

To determine the stability of the column under the application of relatively high pulsed currents, the CVFI prototype was used as a series circuit element in the IND-1 charging circuit. The column used for these tests was about 10 cm long and slightly greater than 3 mm in diameter. Current risetime was about 2.2 msec with the maximum current determined by the capacitor bank voltage. Charging the IND-1 at 1 kv which corresponds to approximately 520 amps resulted in no observable instabilities, even when the storage inductor was crowbarred at peak current. It was found that, when using the crowbar, the current limit was about 870 amps at which point instabilities would occur occasionally. At currents of 1000 amps instabilities were consistently observed. At this current, self-interruption of the CVFI, when used to switch current into a 1 ohm load, produced energy transfers of about 15% to the load. This compares favorably with the self-interruptions of the MSI-3 which, at atmospheric pressure and mercury as the interrupting medium, achieved only 10% into .42 ohm load.

One fact worth noticing regarding the mechanical stability of the columnar flow in mercury is that the Reynolds number R_p is relatively high

$$R_p = v d \rho / \eta \quad (1)$$

where $\rho = 13.6$ grams/cm³; $\eta = 1.7 \times 10^{-2}$ poise; $d \cong 3$ mm, and a reasonable estimate for v is 10 cm/sec. R_p is then 2400.

The transition from laminar flow to turbulent flow takes place at $R_p = 2100$ to 4000, so we are in that range. Judging from photographs of the column, however, with a column length of 10 cm, or less, inherent mechanical instabilities were not present.

To demonstrate the powered mode interruption, the column of mercury was allowed to pass through the bore of a coil which was somewhat unsuited for this application. The circuitry used in this experiment is shown schematically as Fig. 40. The bore length of the coil was 3". Ideally, the coil should have a bore length of the same order of magnitude as the column diameter (1/4" or less) to concentrate the magnetic force on just a small section of the column. Even so, results of the experiment proved to be rather good (see Fig. 41). When the trace of the oscillogram is along the zero line, the switch is open. The 60 cycle pickup shown in the oscillogram is from the antenna effect of our observational circuitry. The "open time" observed (60 - 80 msec) agreed well with the calculated fall time of the mercury from the coil center to the lower reservoir.

In addition to the experimentation above, external pulsed magnetic fields were also applied to the liquid column when used in the IND-1 circuitry. The applied fields were of several different geometrical configurations, corresponding to the various driver coils that have been used in conjunction with this switch.

The first type of external \bar{B} field was generated by a pancake coil magnet with an opening in its center about 3/4" long and 1/4" in diameter.

As in the preliminary testing of the CVFI, the free-falling liquid metal was passed through the bore of the magnet. Results conclude that the external magnetic field in this case did not appreciably affect the interruption (see Fig. 42). Indeed, in some interruptions the application of the magnetic field of this coil appeared to lower the energy switching efficiency from that observed without the applied field (i.e., self-interruption).

It should be noted that in these experiments we have been using currents through the CVFI that are themselves sufficient to produce self-interruptions. The general procedure has been to measure the voltage and energy delivered to the load with the self-interruption process and then with all other parameters held constant, apply the external magnetic field and compare the resultant voltage and energy with that previously described. From this method the effectiveness that the external field lends to the interruption process can be determined.

A second type of external field was applied from a magnet in the form of a Helmholtz pair. Figure 43 shows the magnitude of the horizontal \bar{B} field of the coils and the orientation of the mercury column with respect to the coils. It was found by use of magnetic field probes that the \bar{B} field through which the liquid column passed was about 1600 gauss per kilovolt potential stored on the 28 μf capacitor bank used to energize the magnets. Results of this experiment indicate only a slight improvement over the self-interruption mode. It was decided from this procedure that a stronger magnetic field was needed to produce a significant improvement in energy transfer.

The next step in the direction of stronger field density was the utilization of a laminated iron C-core pulse magnet. Design of this magnet used a continuous strand of RG-58 center conductor, wound 90 times radially around the core (Fig. 44), giving a field geometry described in Fig. 45. It was found that for 1 kv bank voltage (28 μ f), a \bar{B} field of 6200 gauss was produced perpendicular to the liquid column. In this case, as well as that of the Helmholtz pair geometries, the force exerted on the current carrying column is essentially a $\bar{I} \times \bar{B}$ force which tends to move the whole column rather than to reduce its diameter by the field gradient within the conductor itself as the pancake coil is designed to do. Interruption thus occurs because of an initial shearing force on the column which increases the effectiveness of the self-interruption forces.

It is of interest to compute the horizontal velocity imparted to the liquid column by the application of a magnetic field of this type.

The magnetic field acts upon about a 1" section of the flowing column. Then, using the experimental parameters of the column, namely that the liquid is mercury and the column diameter is approximately 3 mm, it is possible to calculate the mass of the mercury that is involved. Since the speed of flow of the mercury is relatively slow with respect to the duration of the magnetic field, it is possible to neglect the flow altogether. The mass affected will then be just the mass of mercury in the 1" segment.

$$M = r^2 l \rho \cong 2.5 \text{ grams} \quad (2)$$

where $r = .15$ cm, $\ell = 2.54$ cm, and the density $\rho = 13.7$ grams/cm³.

Using the above result and the equation

$$\int F dt = m(\Delta v) \quad (3)$$

where F is given by

$$F = I(\bar{\ell} \times \bar{B}) = I\ell B_{\max} \sin \omega t \quad (4)$$

since $\bar{\ell}$ and \bar{B} are perpendicular. Due to the high inductance of the C-90 magnet, it was possible to prevent backswing of the discharge pulse because of ignitron cut-off (Fig. 46). In this interruption scheme this is very desirable in that no opposite swinging B-field is set up to oppose the initial velocity imparted to the mercury column.

Since the initial horizontal velocity of the mercury column is zero, we can solve Eqs. (3) and (4) for v_h , the final horizontal velocity

$$v_h = (1/M) \int_0^{\pi/\omega} F dt = (1/M) (B_{\max} I \ell) \int_0^{\pi/\omega} \sin(\omega t) dt \quad (5)$$

where we are integrating over a 1/2 cycle since there is no backswing. Then

$$\begin{aligned} v_h &= (B_{\max} I \ell / M)(2/\omega) \\ v_h &= (B_{\max} I \ell / M)(\tau / \pi) \end{aligned} \quad (6)$$

Then with 1 kv on the IND-1 charging bank, $I \cong 520$ amps, and 1 kv on the driver bank corresponds to .62 webers/m², and τ as seen from the field oscillographs is

about .4 msec.

$$v_h = \frac{(.62 \text{ webers/m}^2)(520 \text{ amps})(2.54 \times 10^{-2} \text{ m})(.4 \times 10^{-3} \text{ sec})}{2.5 \times 10^{-3} \text{ kg (3.14)}} \quad (7)$$
$$v_h = .42 \text{ m/sec}$$

An example of the interruption produced with the C-90 coil geometry is shown in Fig. 47. Although the efficiencies are relatively low, they compare favorably with the atmospheric pressure results with the MSI-3 and MSI-4, indicating that the CVFI promises even higher efficiencies in an elevated pressure environment.

Preliminary work has also been performed using two C-90 coils to drive sections of the column in opposite directions, thus increasing the shearing action (Fig. 48). Interruption data is still incomplete for this coil configuration, but theoretically, switching efficiencies should certainly increase.

References:

- ¹Advanced Kinetics, Inc., Technical Documentary Report, "Inductive Storage Switch Study" Contract No. AF30(602)-3512, Rome Air Development Center, July, 1965.
- ²H. P. Furth, R. W. Waniek, Rev. Sci. Instr. 27, 195 (1956).
- ³Marshall Sittig, Sodium (Its Manufacture, Properties and Uses) (Reinhold Publishing Corp., New York, 1956).
- ⁴Advanced Kinetics, Inc., Technical Documentary Report, "Inductive Storage Switch Study" RADC Contract No. AF30(602)-3512, July, 1965, p. 47.
- ⁵Insulation Directory/Encyclopedia Issue, May-June, 1964

III) CONCLUSIONS

The interrupter studies conducted at Advanced Kinetics, Inc. during the past two years have been guided by the concept of using the pressure of strong pulsed magnetic fields to produce very rapid mechanical interruption. This basic concept has proved to be a sound one. As a result of our research, we have added a second concept which turns out to be equally basic in all applications where the interruption is to be repetitive, especially at high repetition rates. This is the concept of using liquid metal as the mechanical element, and to arrange to have the interruption occur between two sections of the liquid.

There are two over-riding advantages in liquid-to-liquid interruption:

1. There is no erosion of electrode surfaces, which we have found to be inevitable in solid mechanical interrupters and liquid-to-solid interrupters.
2. The substantial energy which is inevitably deposited in the interrupter element in the form of heat is easily removed by circulating the liquid metal through a heat-exchanger.

These two advantages of liquid-to-liquid interruption are so important for high-powered, high-repetition-rate work that one may consider this approach to preempt completely the area of high-speed mechanical interruption. Initial experimentation with the liquid-to-liquid approach has proved highly encouraging. Future research should be concentrated entirely on this line of progress and should seek to develop present experimental systems toward practical interrupter units of high performance

and reliability.

This development effort will be very much aided by the fact that the theory of magnetic field interaction with conducting fluids (the magnetohydrodynamic theory) is well worked out by now, and is familiar to Advanced Kinetics personnel. In the initial experiments, a correspondence of observed phenomena to hydromagnetic stability theory has already been noted. More sophisticated applications of the theory are planned. Research along these lines will be basic and novel in two senses: from the practical point of view, the liquid-to-liquid method holds unique promise and has never previously been explored by electrical engineers; from the scientific point of view, the study of interruption as an instability phenomenon is of inherent interest to magnetohydrodynamicists.

The most promising specific approach to liquid-to-liquid interruption has turned out to be the use of free-flowing columnar or tubular liquid metal streams. This has the advantage of allowing interruption to take place not only away from solid electrodes, but also away from insulating surfaces which also deteriorate and become overheated. The free-stream approach has the further advantage of causing the interrupter element to reform rapidly (at the stream velocity) and allowing rapid removal of the dissipated heat. The most obvious immediate areas of research are:

1. The maximization of stream velocity and uniformity in the face of ordinary hydrodynamic turbulence and surface tension. This is particularly important for the creation of uniform tubular streams. The

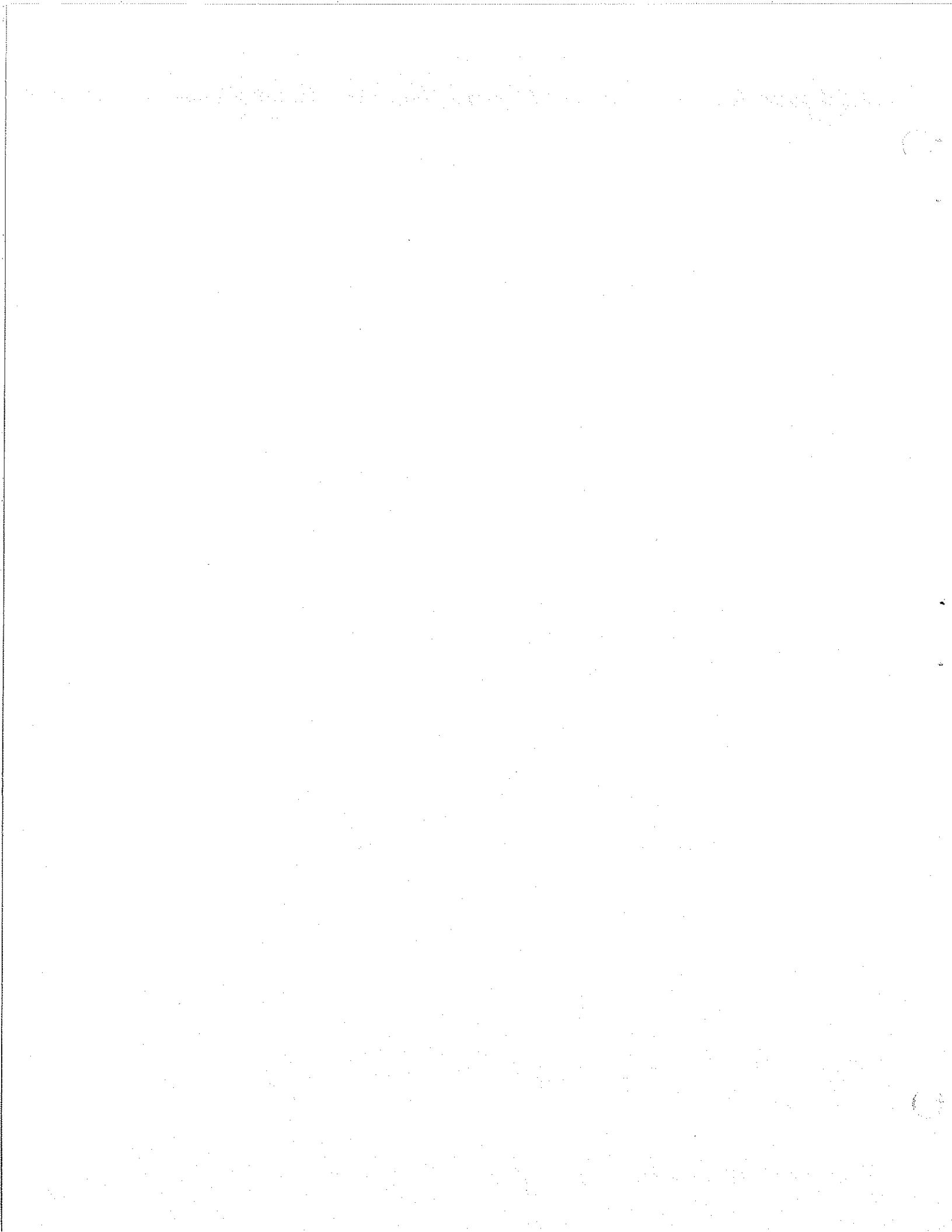
design of the liquid metal nozzle is critical here. The use of interior turbine vanes may yield a significant improvement over simple nozzles.

2. The study of stability of columnar and tubular streams in the presence of large dc currents. The prediction of both ordinary MHD stability theory and finite-resistivity stability theory are clear-cut, promise a highly practical regime of operation, and should be put to a broad experimental test.
3. The optimization of the magnetic trigger element which initiates the instability that interrupts the liquid metal stream. The element needs to be miniaturized and placed in a geometry of maximum effectiveness, so as to minimize the fraction of energy that is lost in initiating the interruption.
4. The maximization of interruption voltage. Useful techniques, such as gas pressurization and multiple interruption, the effectiveness of which we have already demonstrated, needs to be applied to the free-stream interrupter.

By following along the indicated lines of development, an entirely novel and highly effective type of circuit element can be achieved. The hydromagnetically driven liquid-to-liquid interrupter may finally bridge the gap between the solid mechanical and the electronic switches and permit interrupter performance far in excess of what has been possible by other means.

APPENDIX

FIGURES 1 through 48



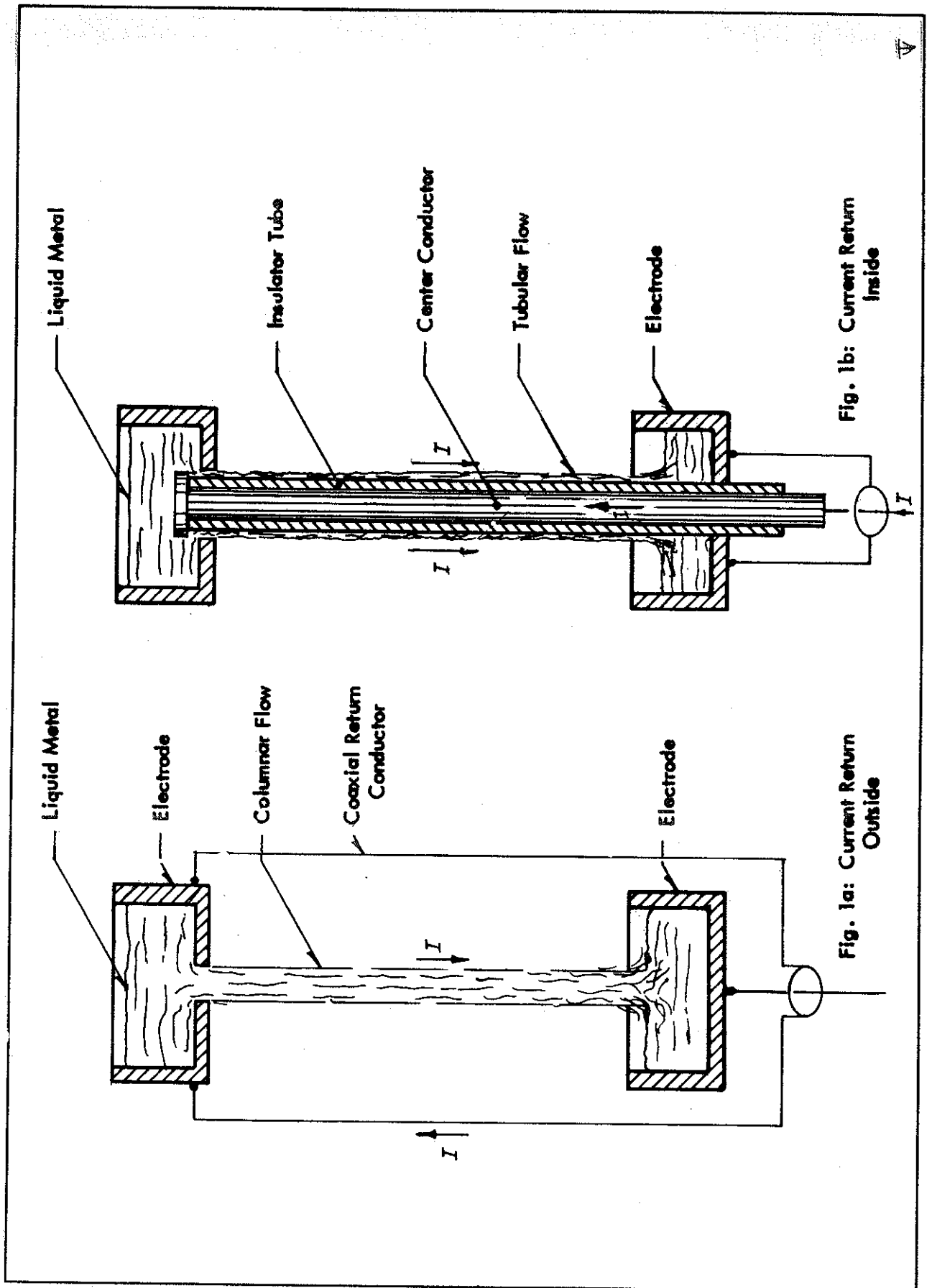


Fig. 1: Coaxial Configuration Incorporating the Flow of Liquid Metal

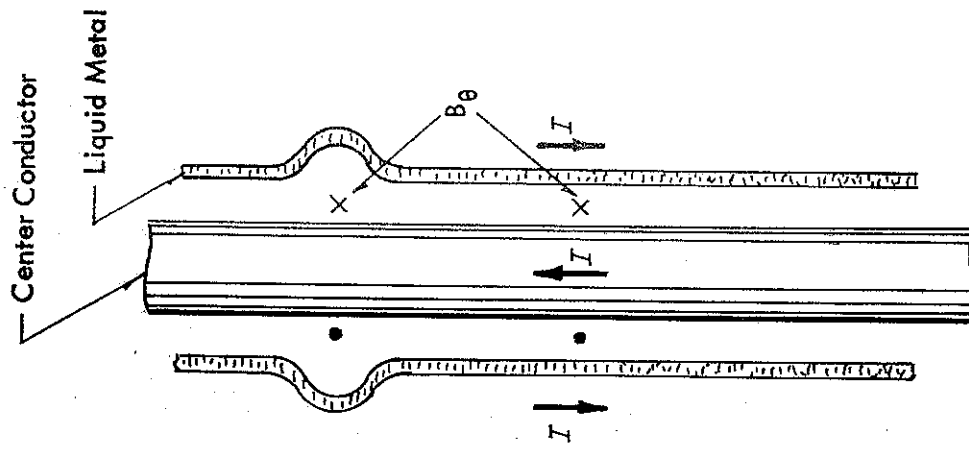


Fig. 2b: Tubular (stable)

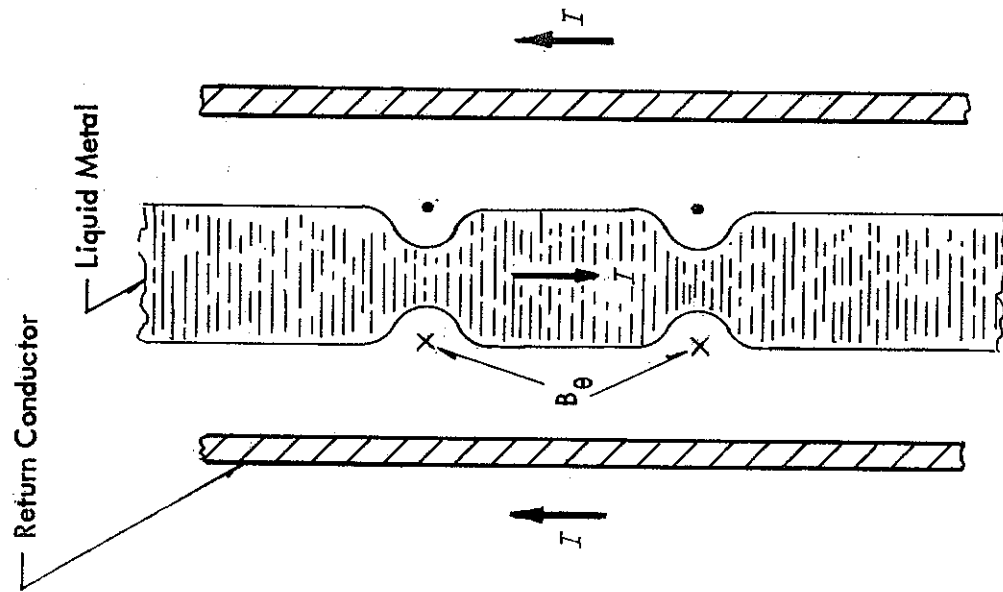


Fig. 2a: Columnar (unstable)

Fig. 2: Perturbations due to the Passage of Current through a Flowing Liquid

Fig. 9: Density as a Function of Temperature for Sodium-Potassium Alloy
(NaK Type 78K - 22Na)

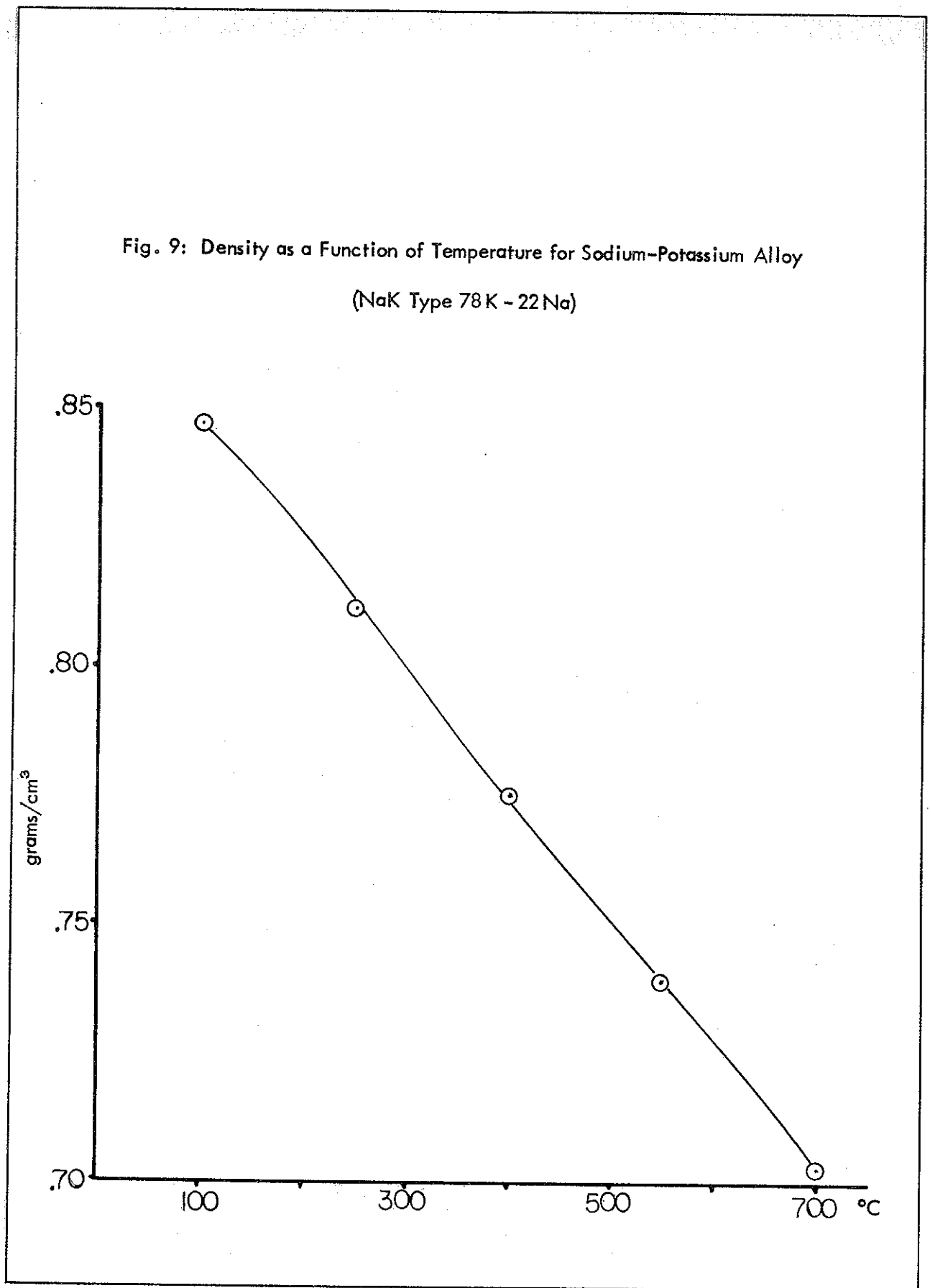


Fig. 10: Density as a Function of Temperature for Gallium

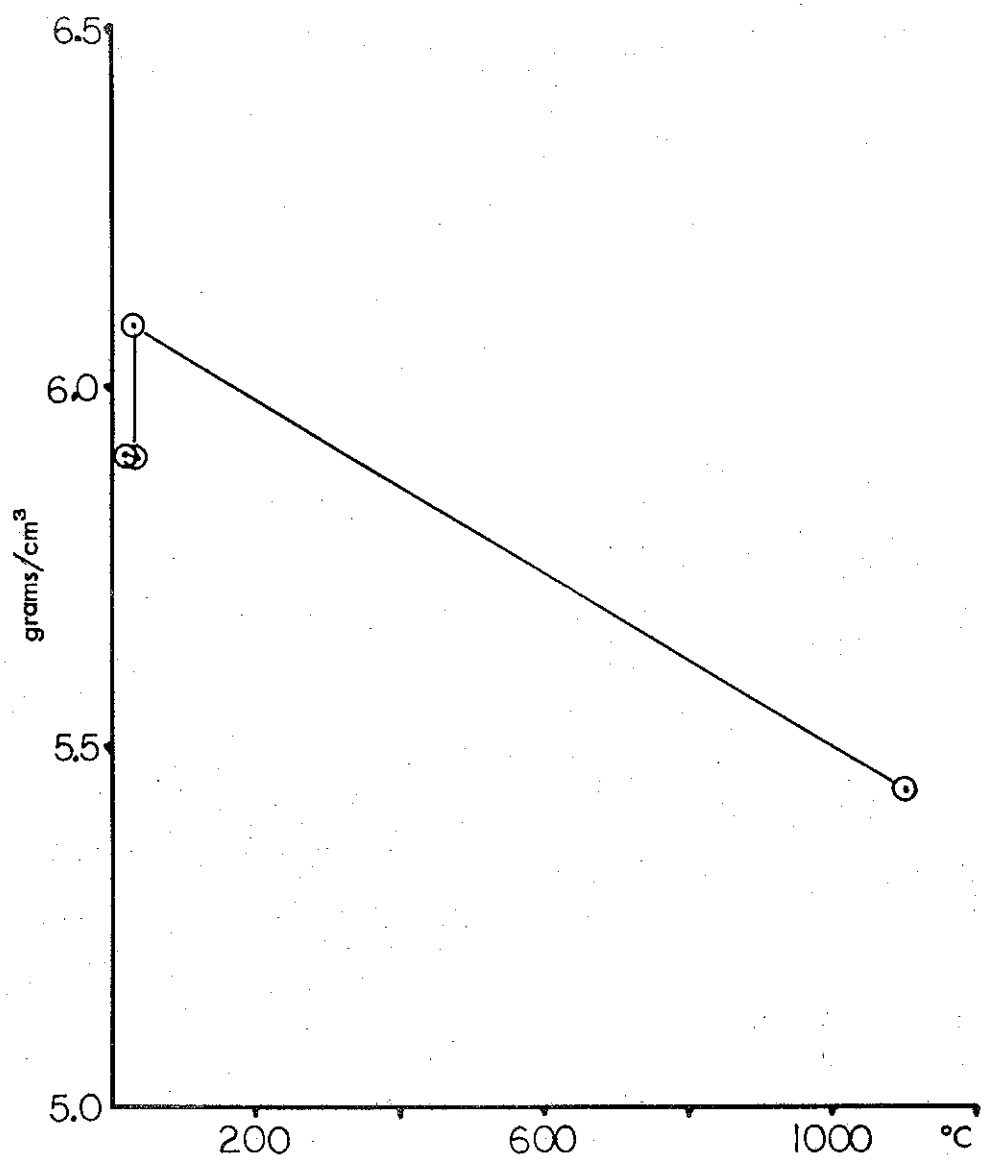


Fig. 11: Density as a Function of Temperature for Mercury

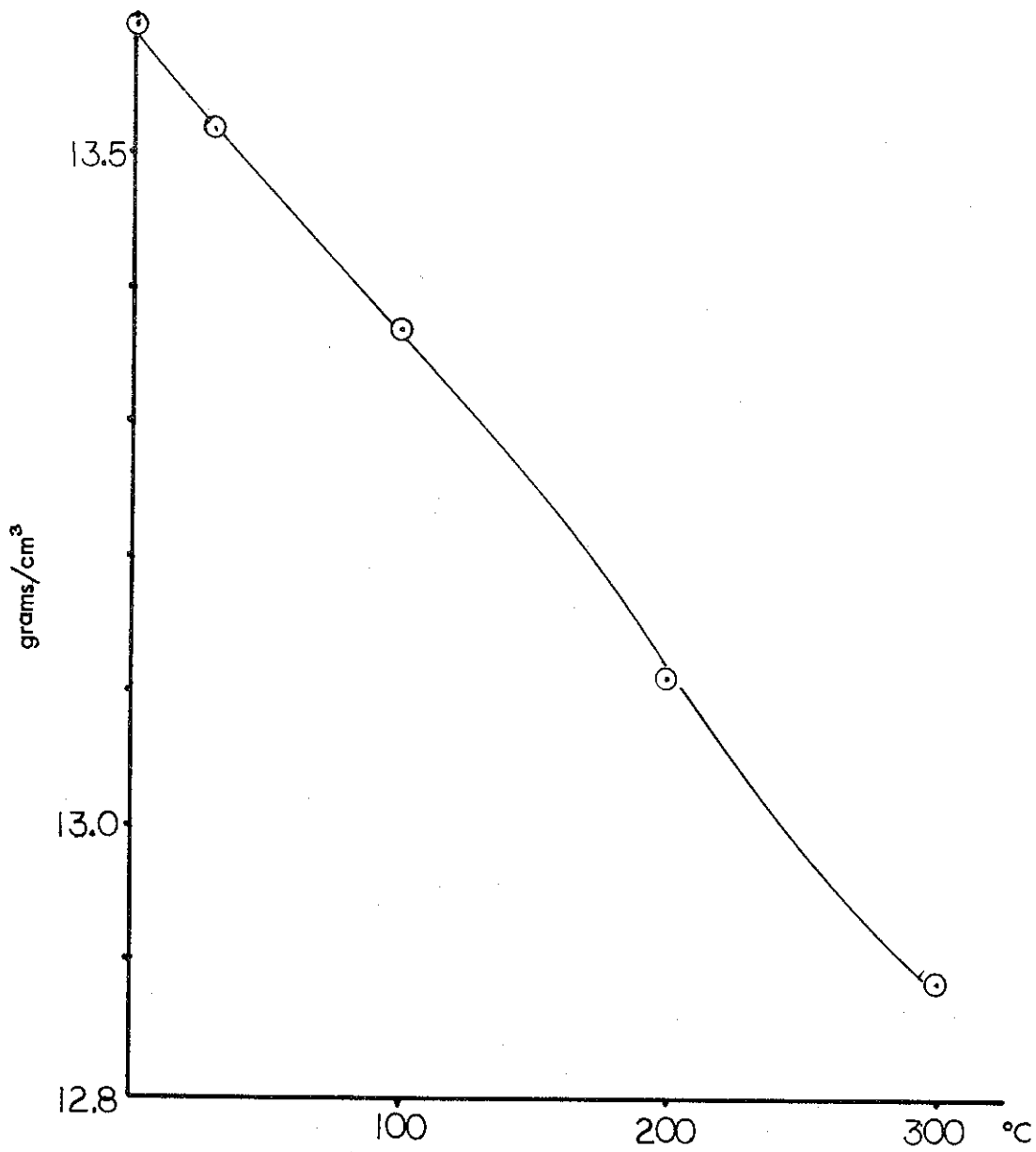


Fig. 12: Electrical Resistivity as a Function of Temperature - Lithium

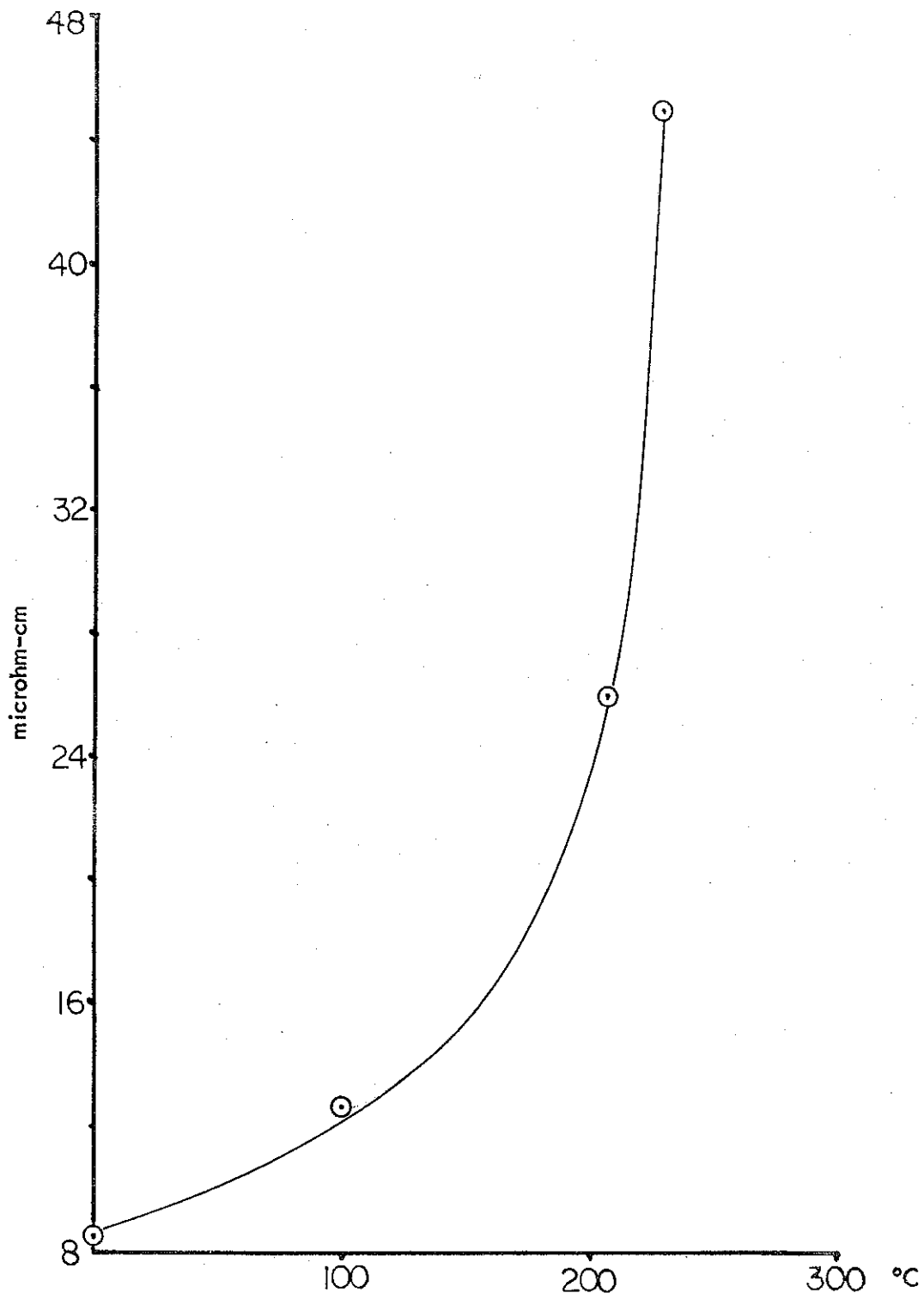


Fig. 13: Electrical Resistivity as a Function of Temperature for Sodium

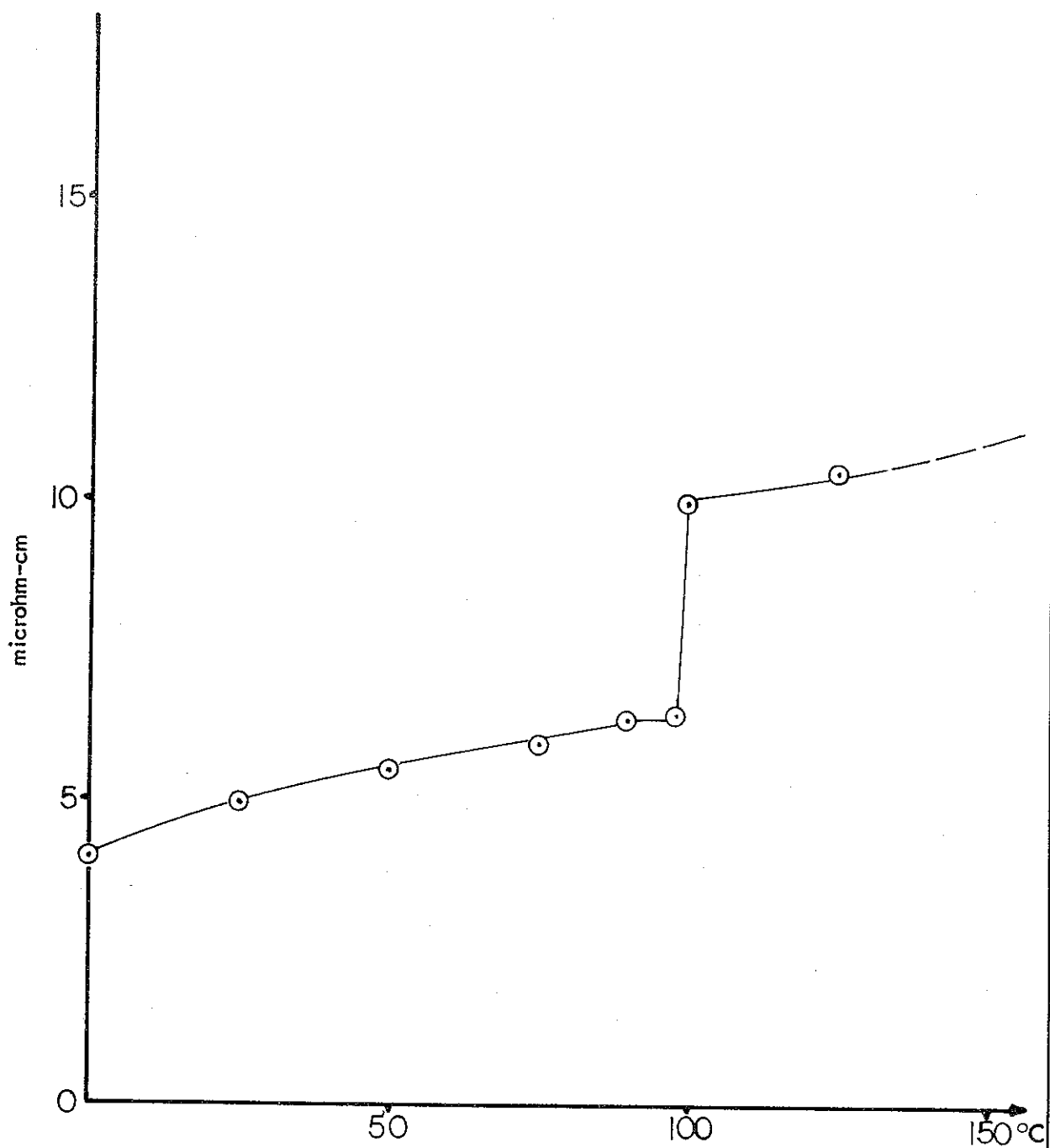


Fig. 14: Electrical Resistivity as a Function of Temperature - Potassium

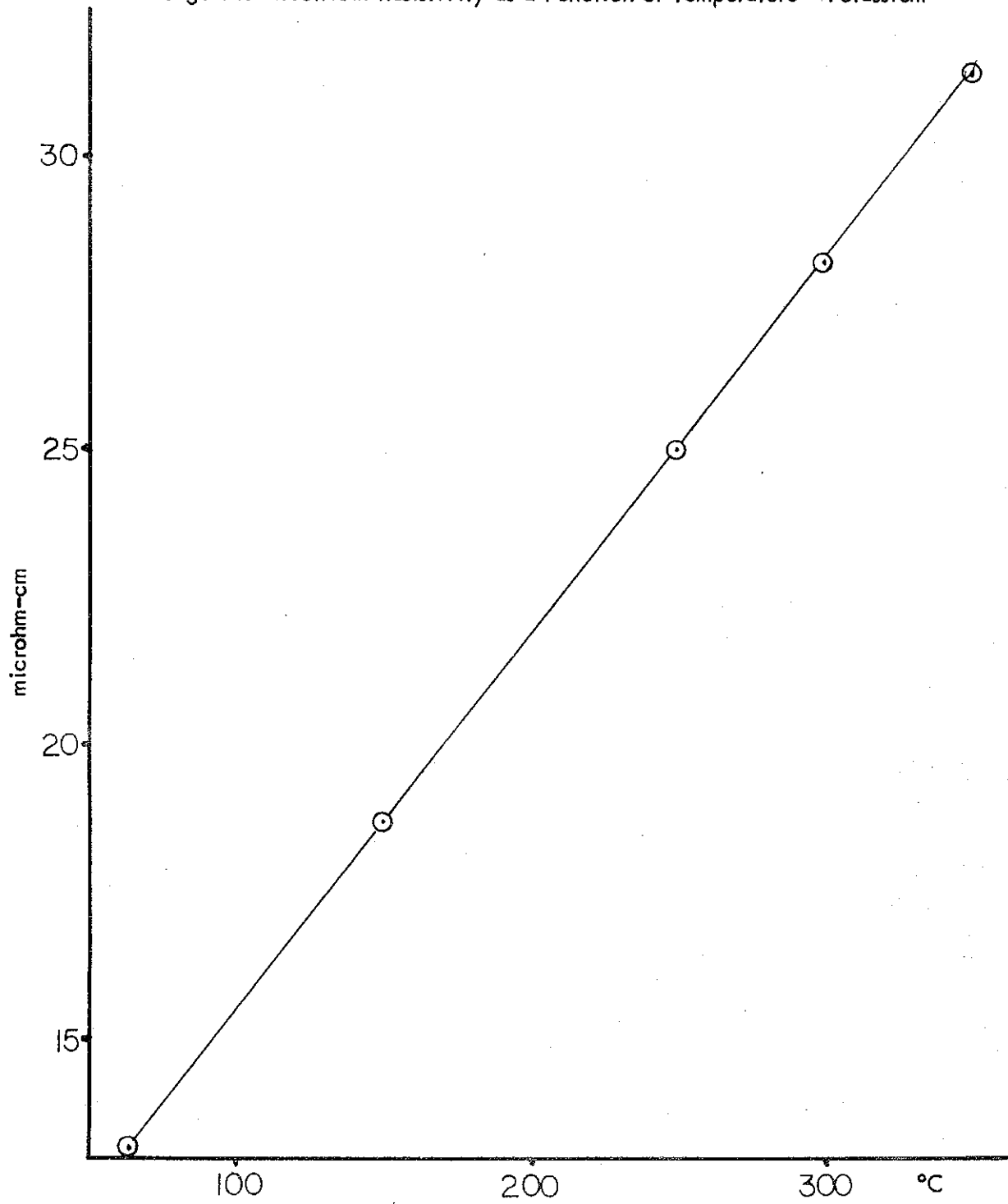


Fig. 15: Electrical Resistivity as a Function of Temperature for Sodium-Potassium Alloy (NaK Type 44K - 56 Na)

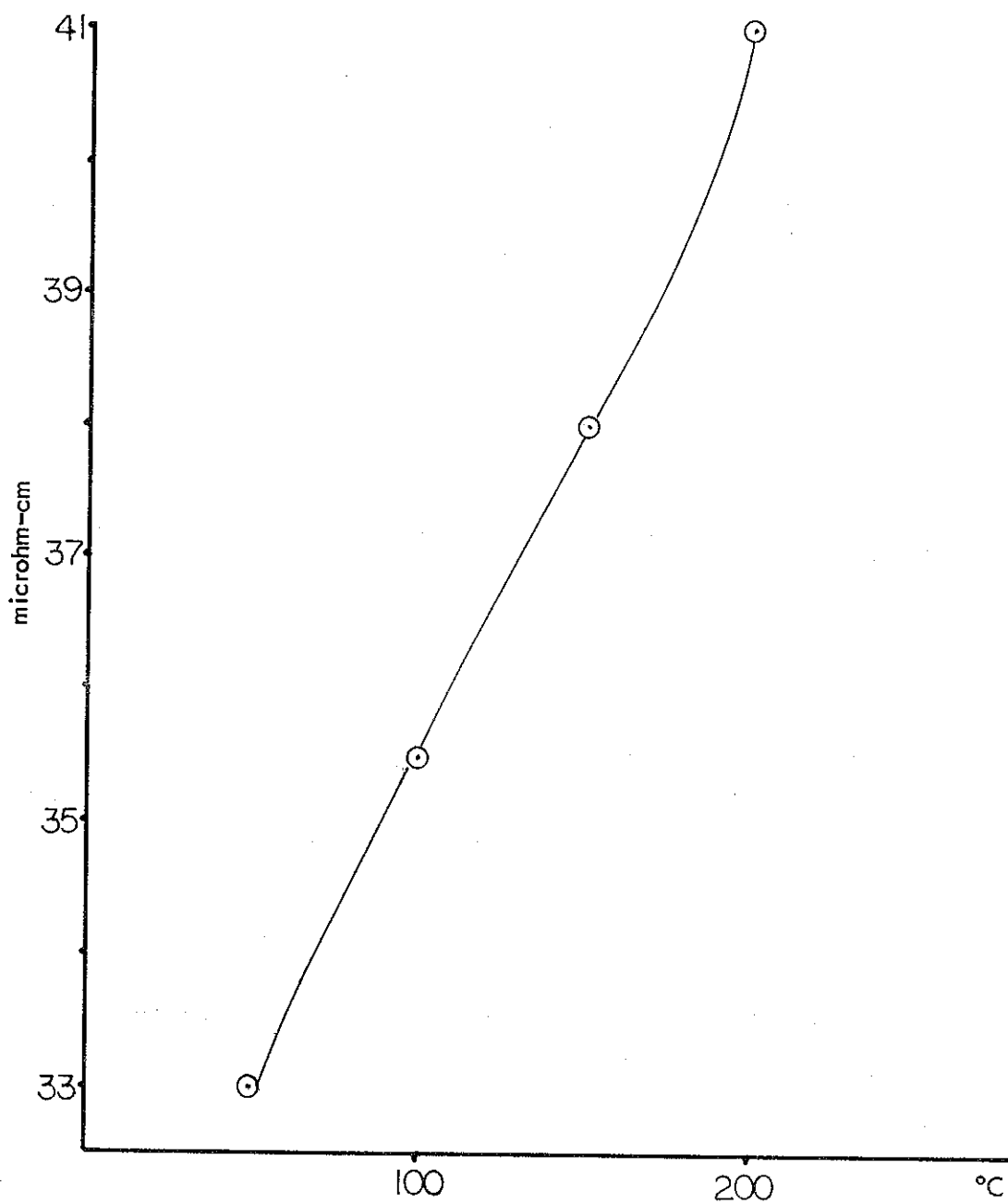


Fig. 16: Electrical Resistivity as a Function of Temperature for
Sodium-Potassium Alloy
(NaK Type 78K - 22Na)

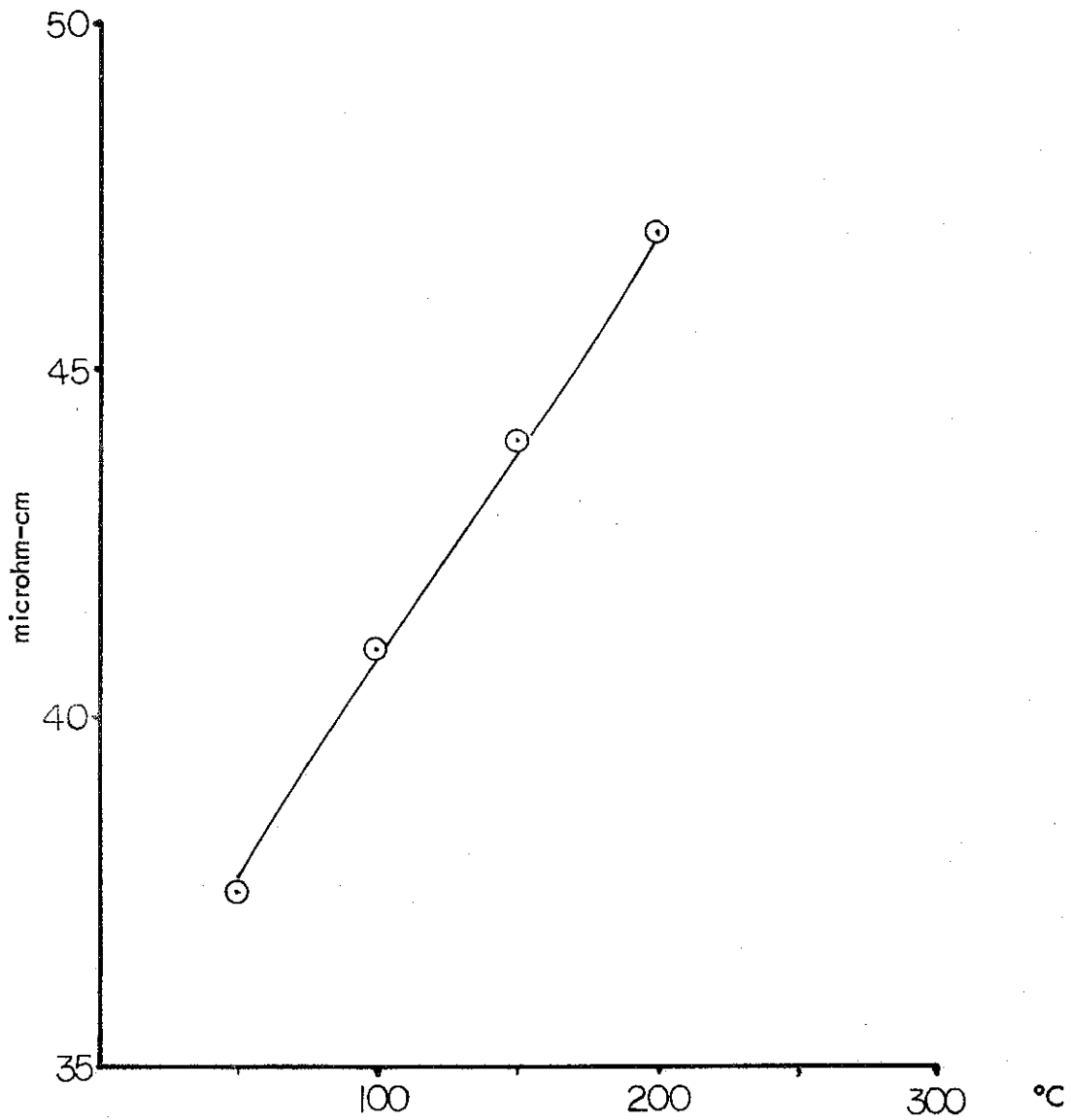
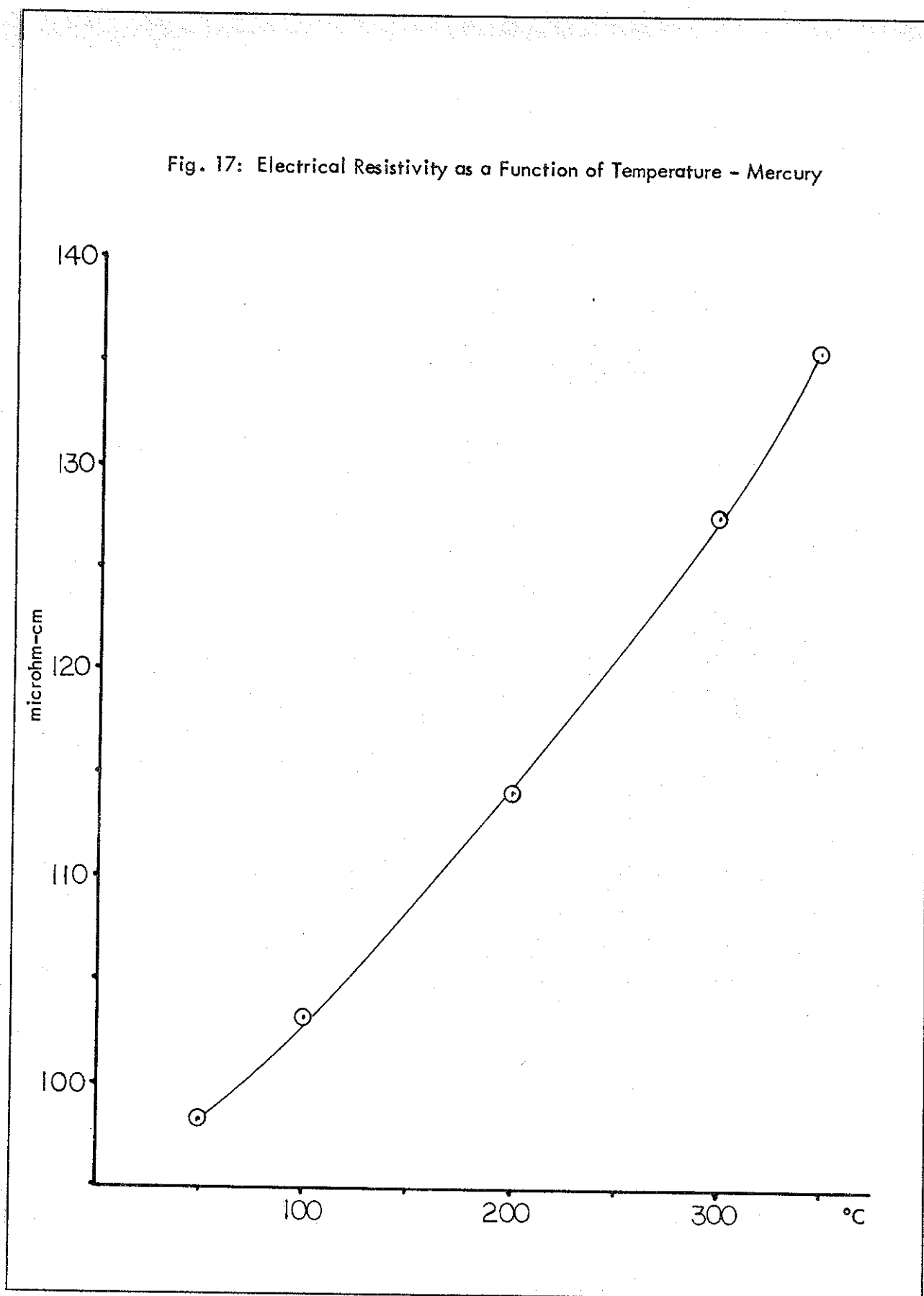


Fig. 17: Electrical Resistivity as a Function of Temperature - Mercury



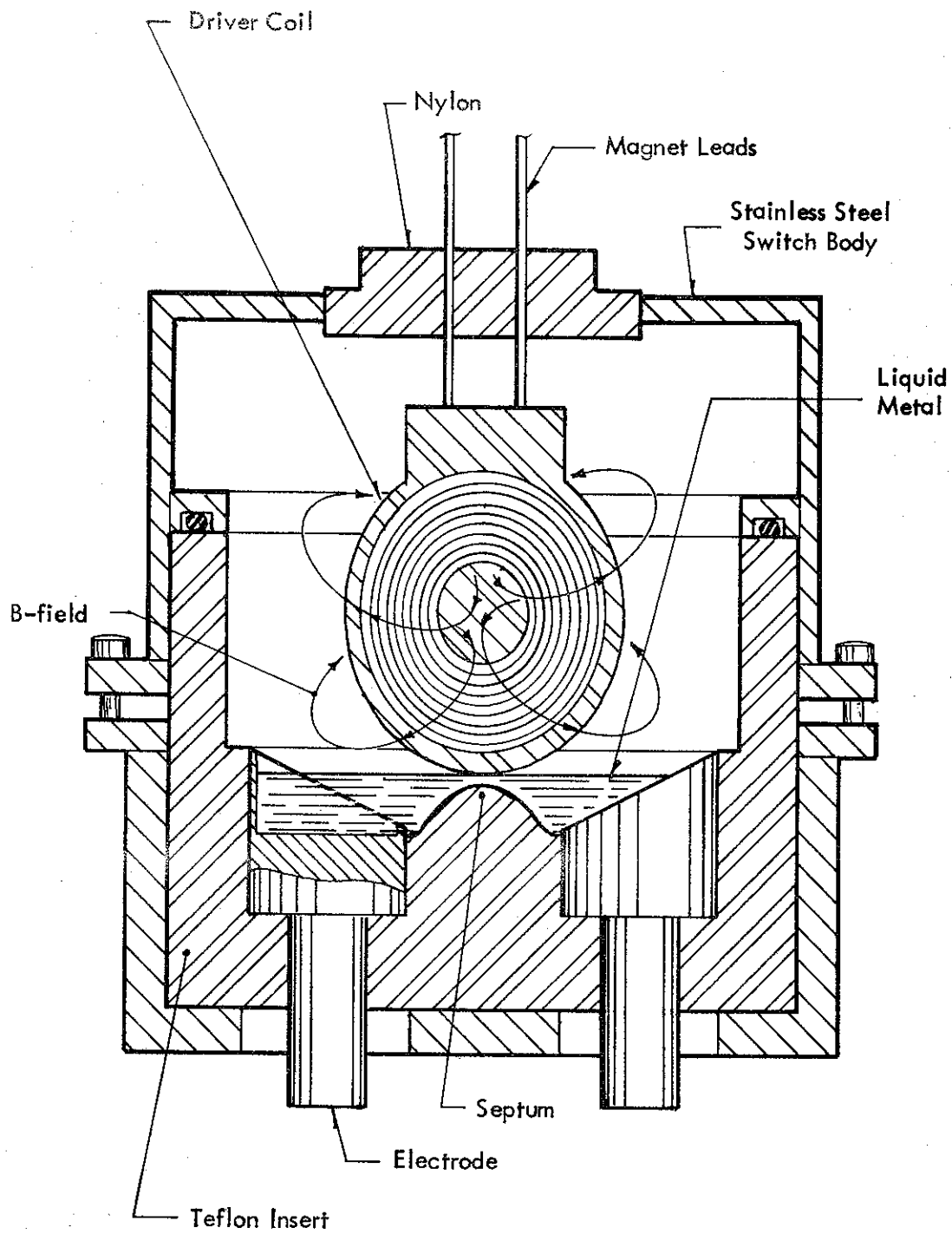


Fig. 18: Cutaway View of the MSI-3

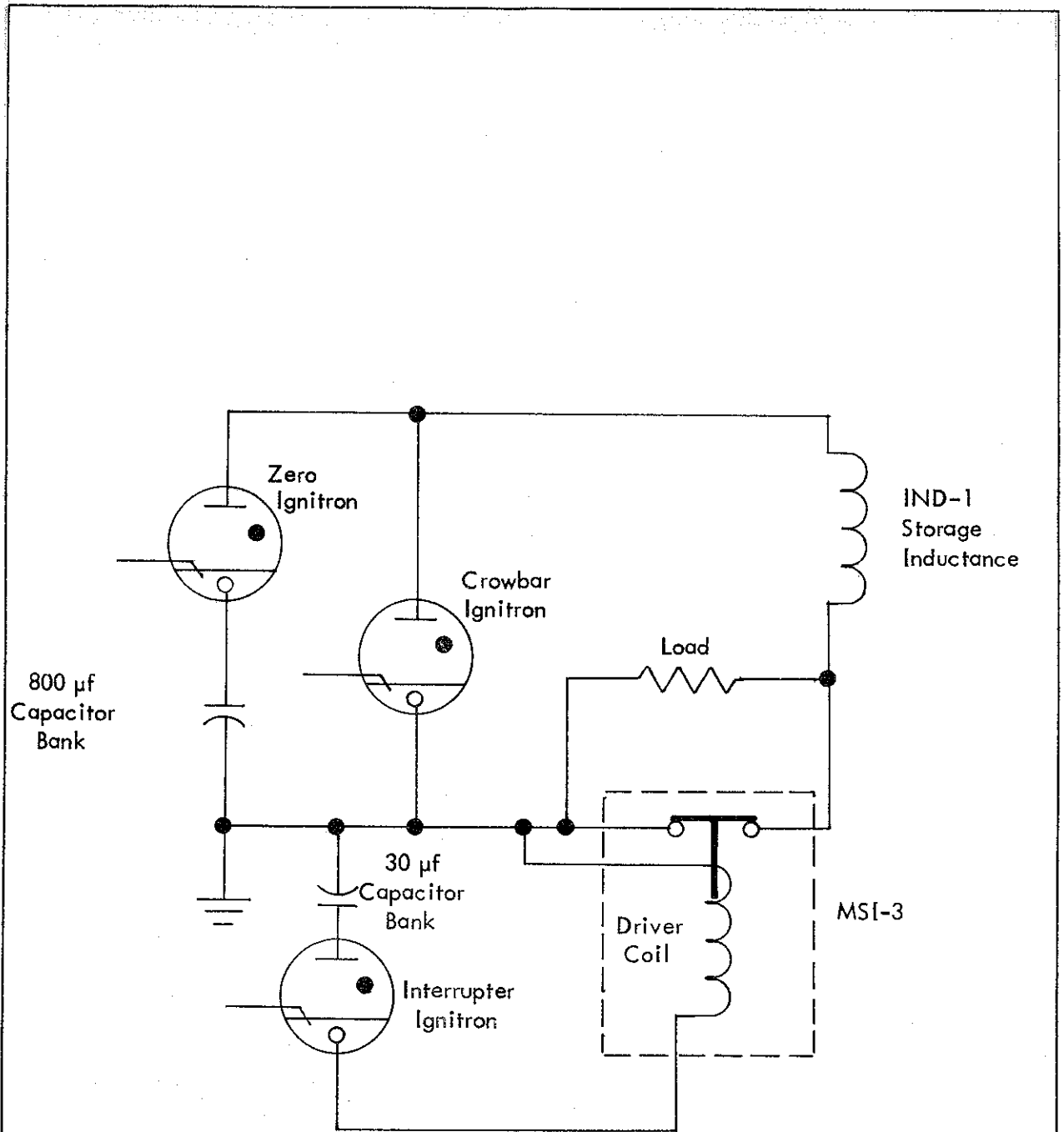


Fig. 19: The MSI-3 Testing Circuitry

An oscilloscope measures voltage across the load during interruption.

Fig. 20: % of Perfect Transfer vs Inductor Current
Using the MSI-3 Self-Interruption Mode
with Atmospheric Pressure Nitrogen in the
Switching Chamber

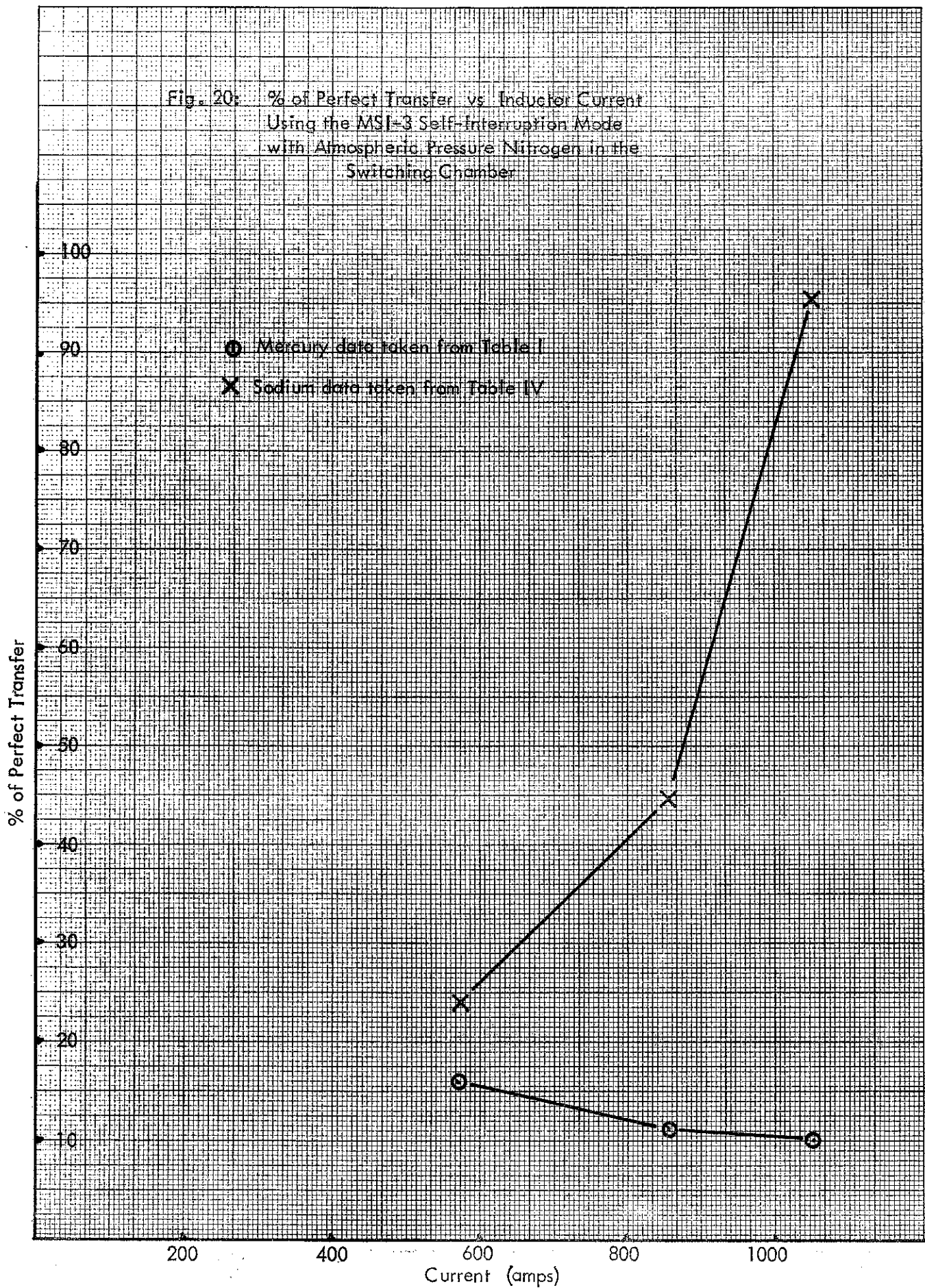


Fig. 21: Dwell Time vs Peak Indicator Current
 Using the MS1-3 Self-Interpretion Mode
 with Atmospheric Pressure Nitrogen in
 the Switching Chamber

○ Mercury data from Table I
 X Selenium data from Table IV

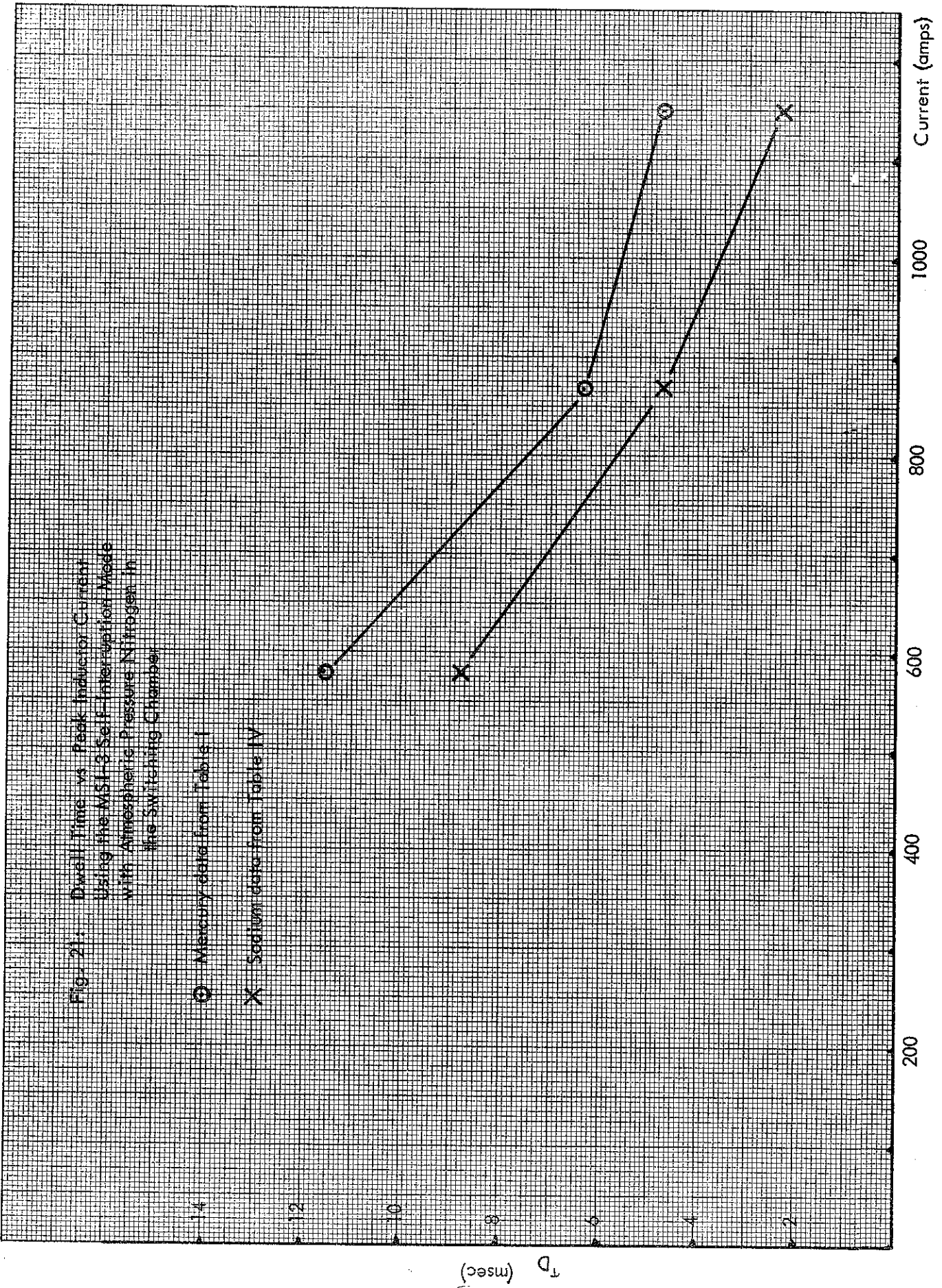


Fig. 22: Arc Duration vs Peak Inductor Current
 Using the MS1-3 Self-Interruption Mode
 with Atmospheric Pressure Nitrogen in
 the Switching Chamber

○ Mercury data taken from Table I

× Sodium data taken from Table IV

Arc Duration (msec)

Current (amps)

14
12
10
8
6
4

200

400

600

800

1000

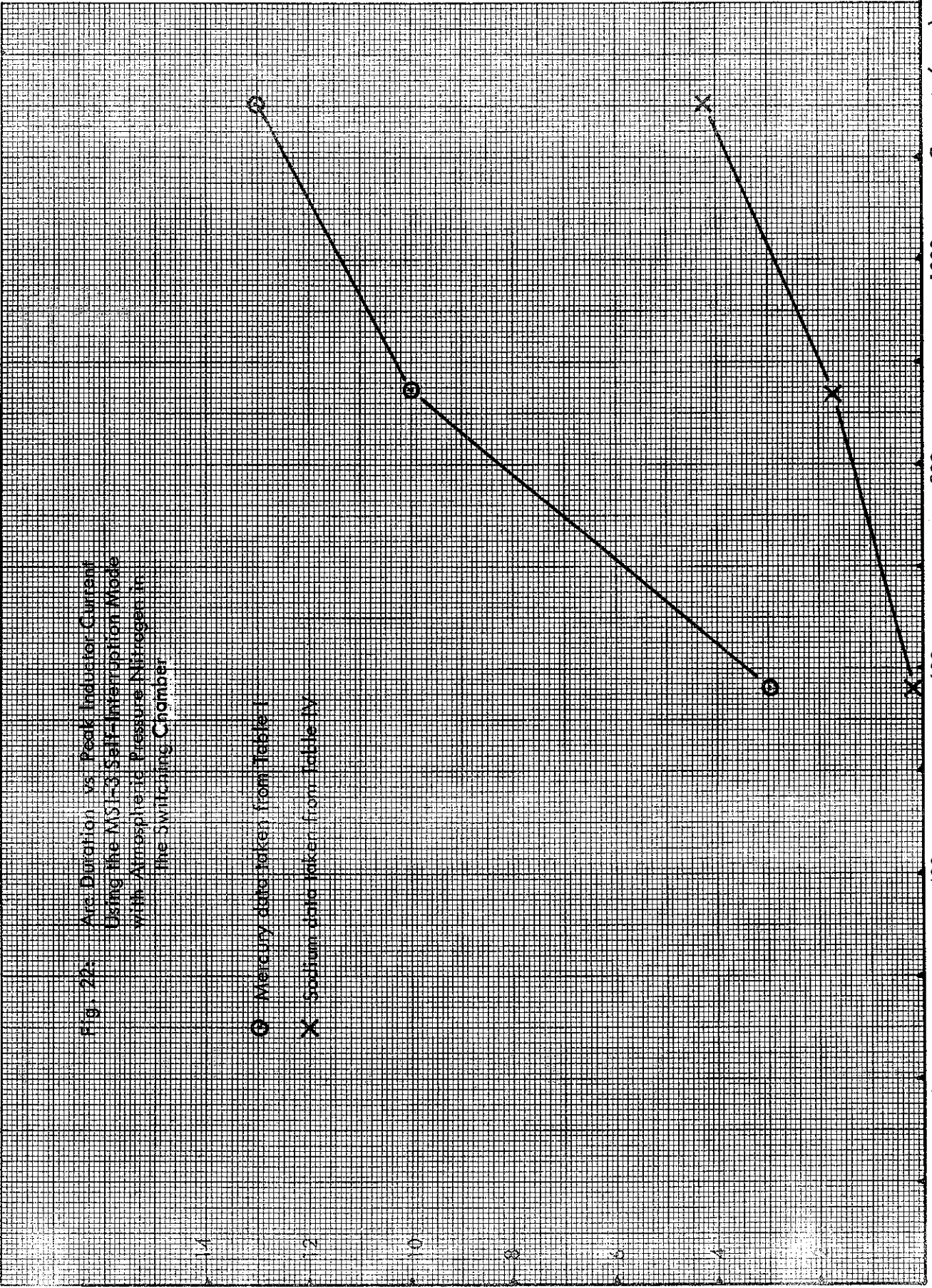


Fig. 23: % of Energy Transferred to Load vs Total Stored Energy Using the MS-3 Self-Interruption Mode with Atmospheric Pressure Nitrogen in the Switching Chamber

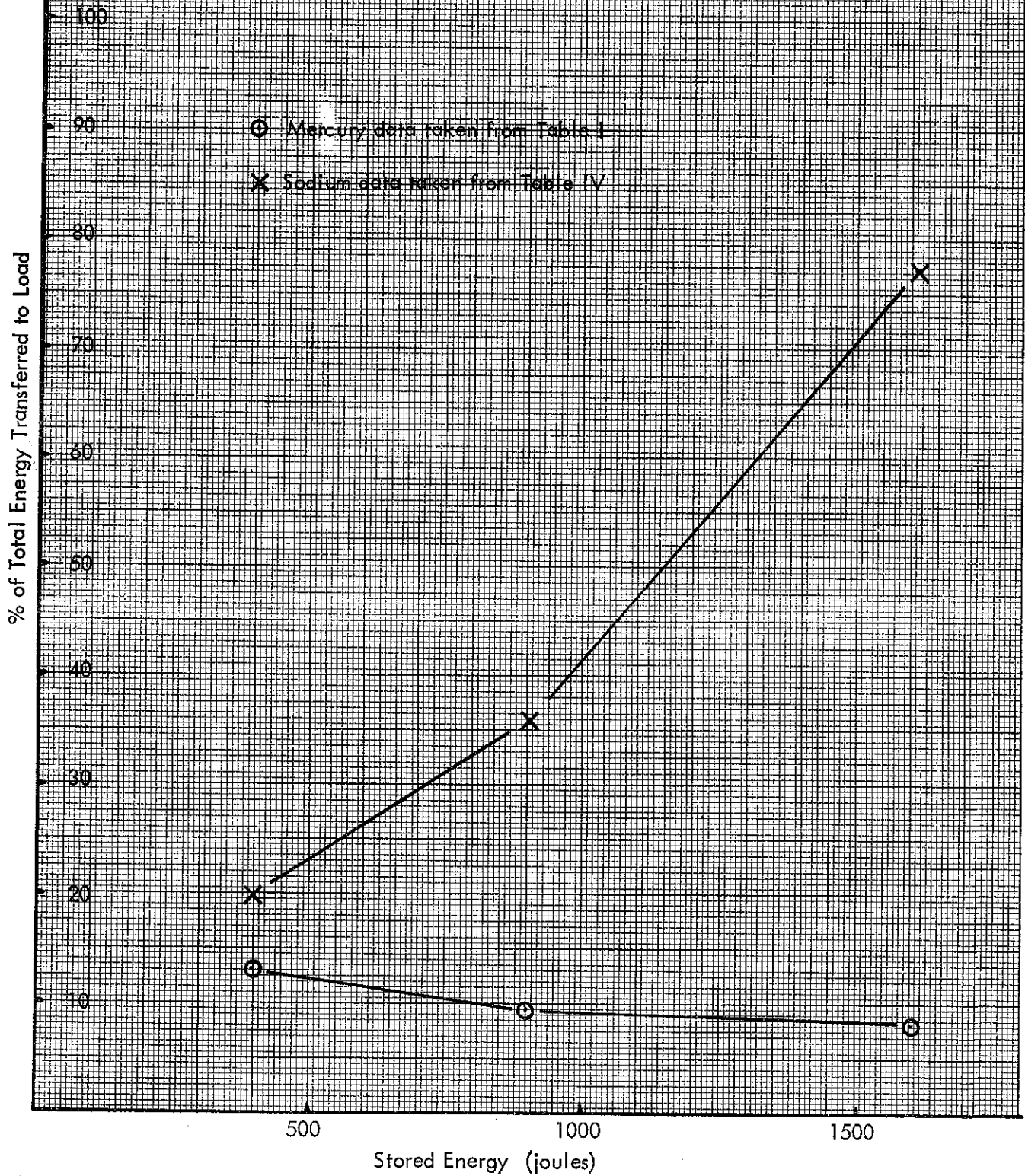
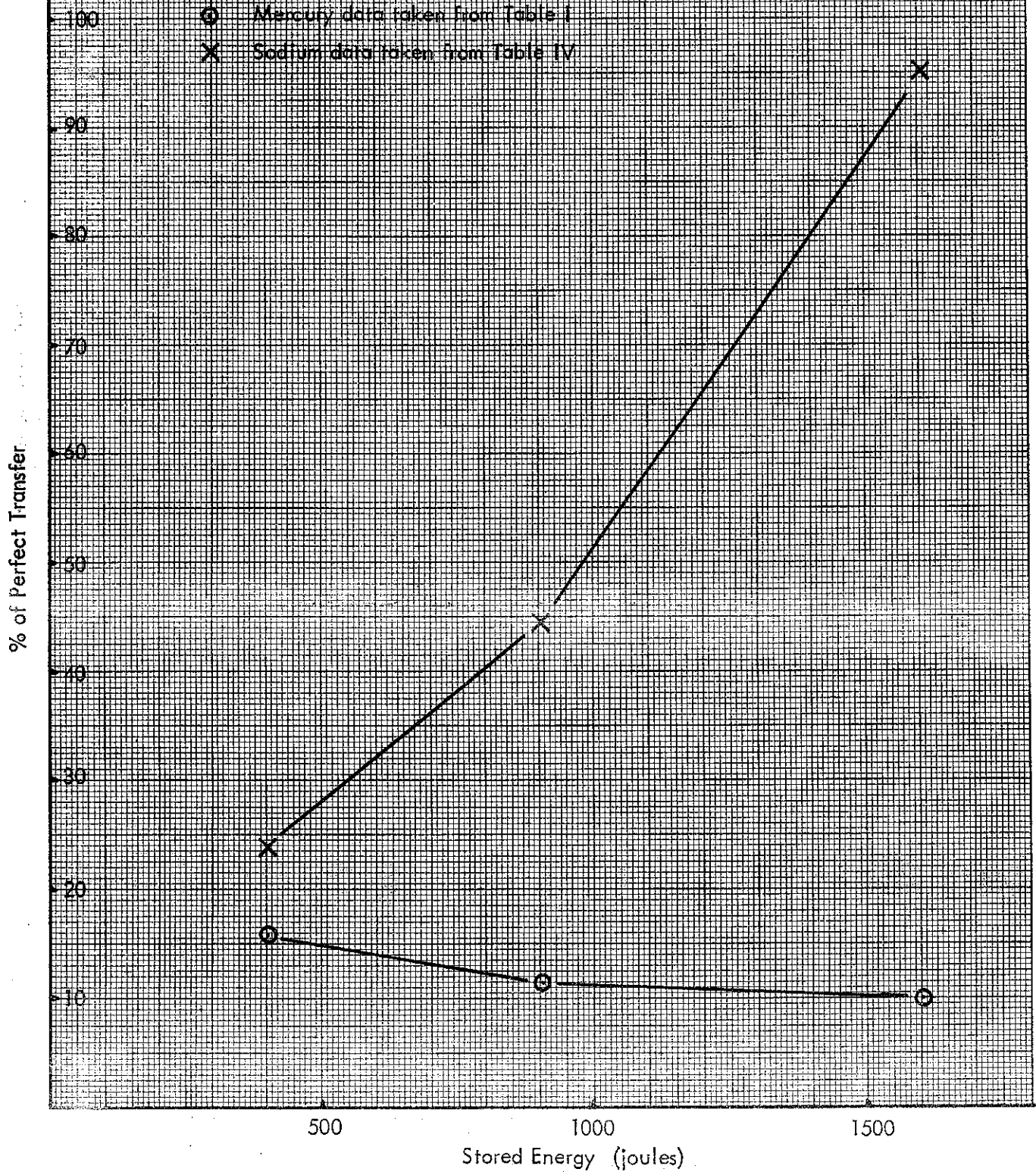


Fig. 24. % of Perfect Transfer vs Total Stored Energy
Using the MSI-3 Self-interruption Mode with
Atmospheric Pressure Nitrogen in the Switching
Chamber



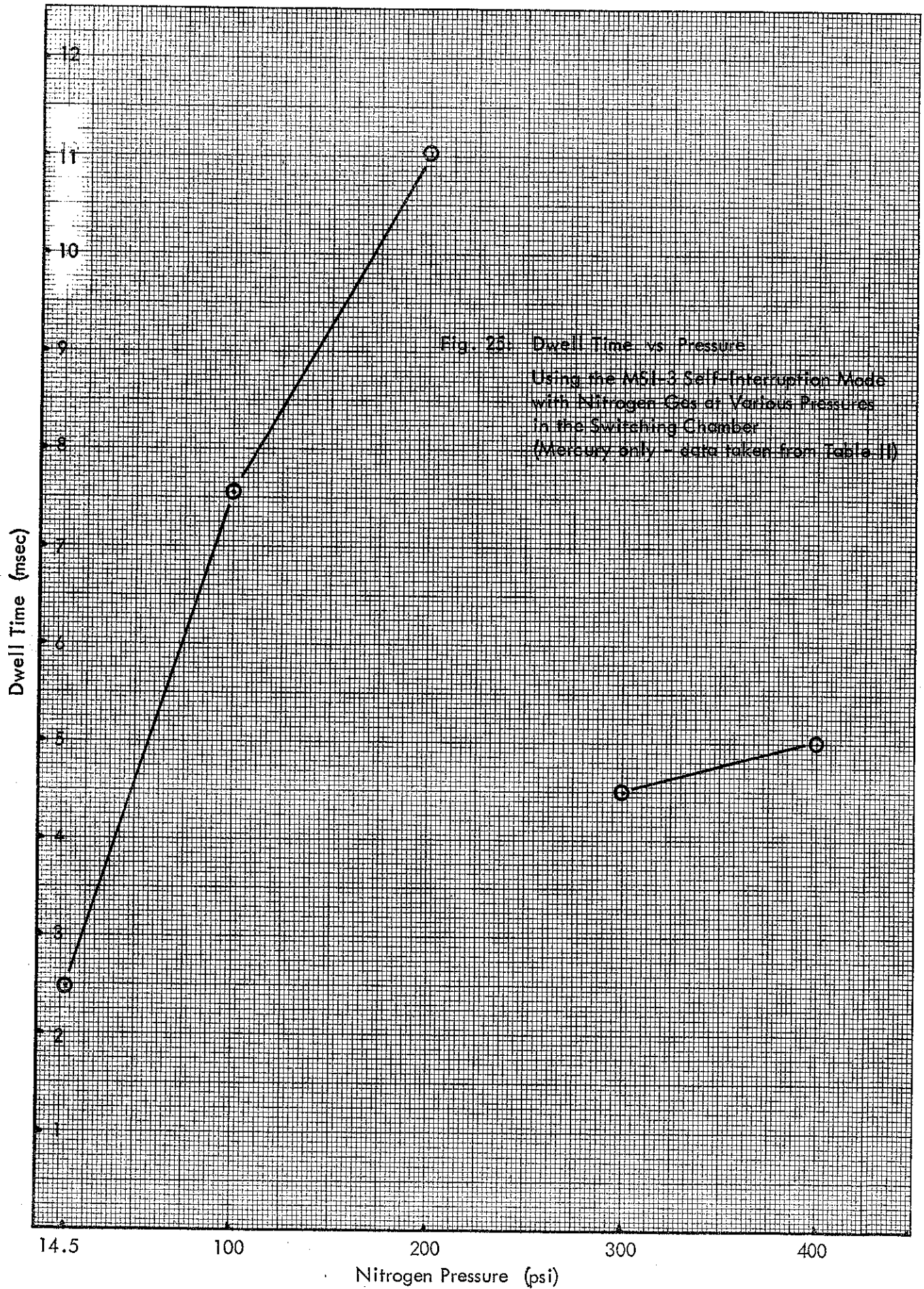
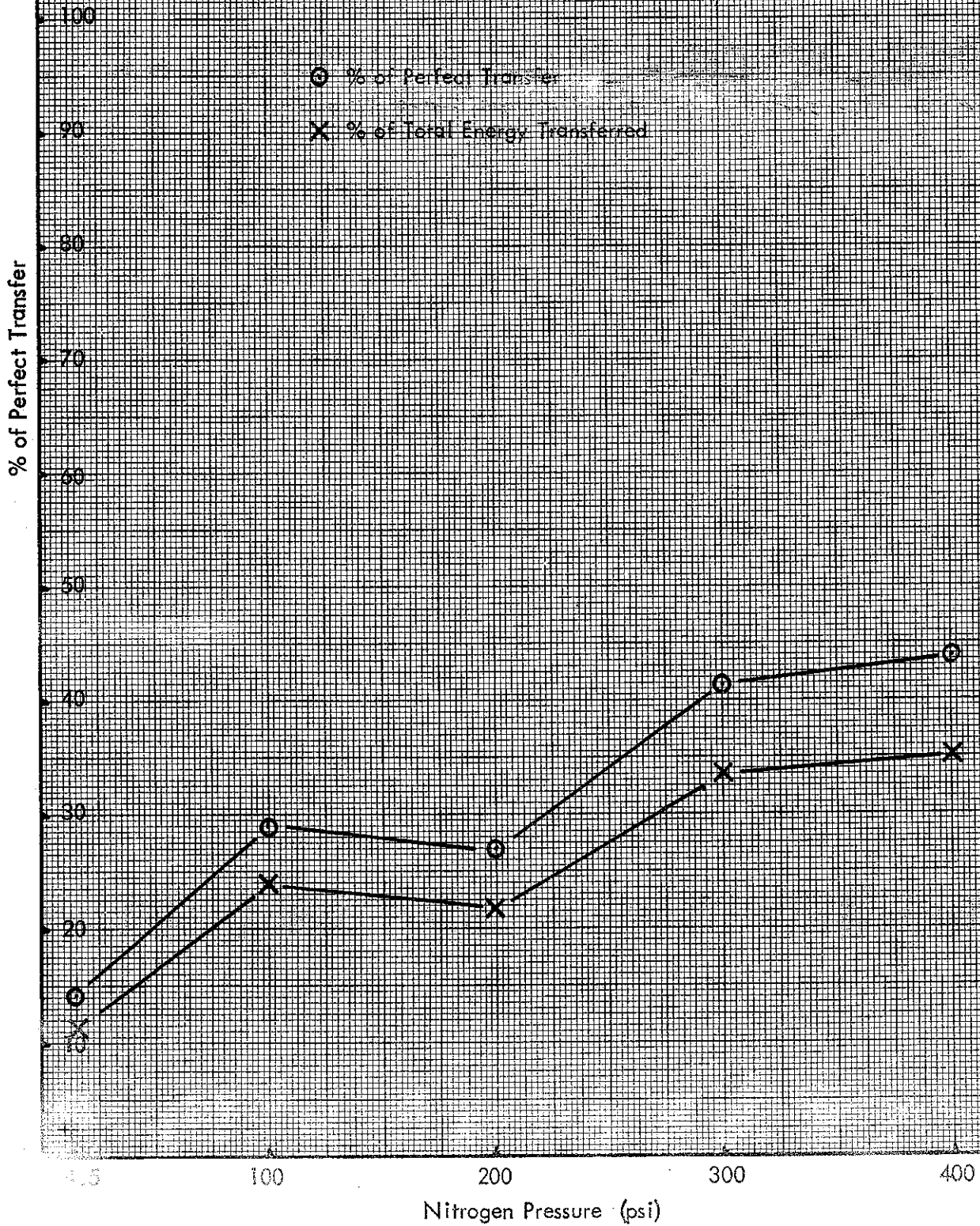


Fig. 25 Dwell Time vs Pressure
Using the MS1-3 Self-Interruption Mode
with Nitrogen Gas at Various Pressures
in the Switching Chamber
(Mercury only - data taken from Table II)

Fig. 26: % of Energy Transfer vs Pressure Using the MS1-3 Self-Interruption Mode with Nitrogen Gas at Various Pressures in the Switching Chamber (Mercury data only, taken from Table I)



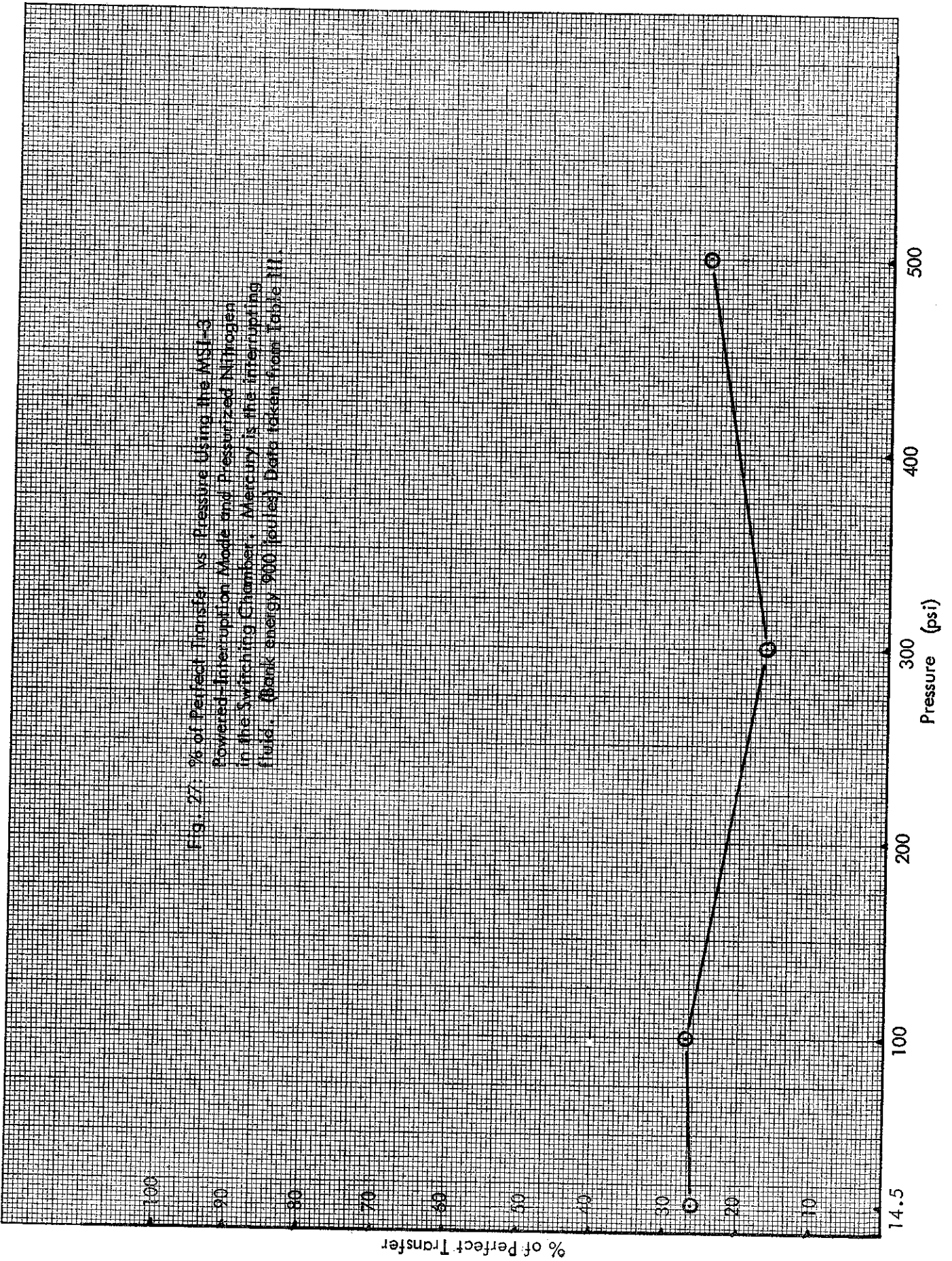


Fig. 27: % of Perfect Transfer vs. Pressure Using the MSI-3 Powered-Interruption Mode and Pressurized Nitrogen in the Switching Chamber. Mercury is the interrupting fluid. (Bank energy 900 joules) Data taken from Table III.

Fig. 26. % of Perfect Transfer vs. Pressure. Using the MS1-8
Powered-Interruption Mode and Pressurized Nitrogen
in the Switching Chamber. Maxey is the interrupting
fluid. (Bank energy 1600 joules) Data taken from Table II.

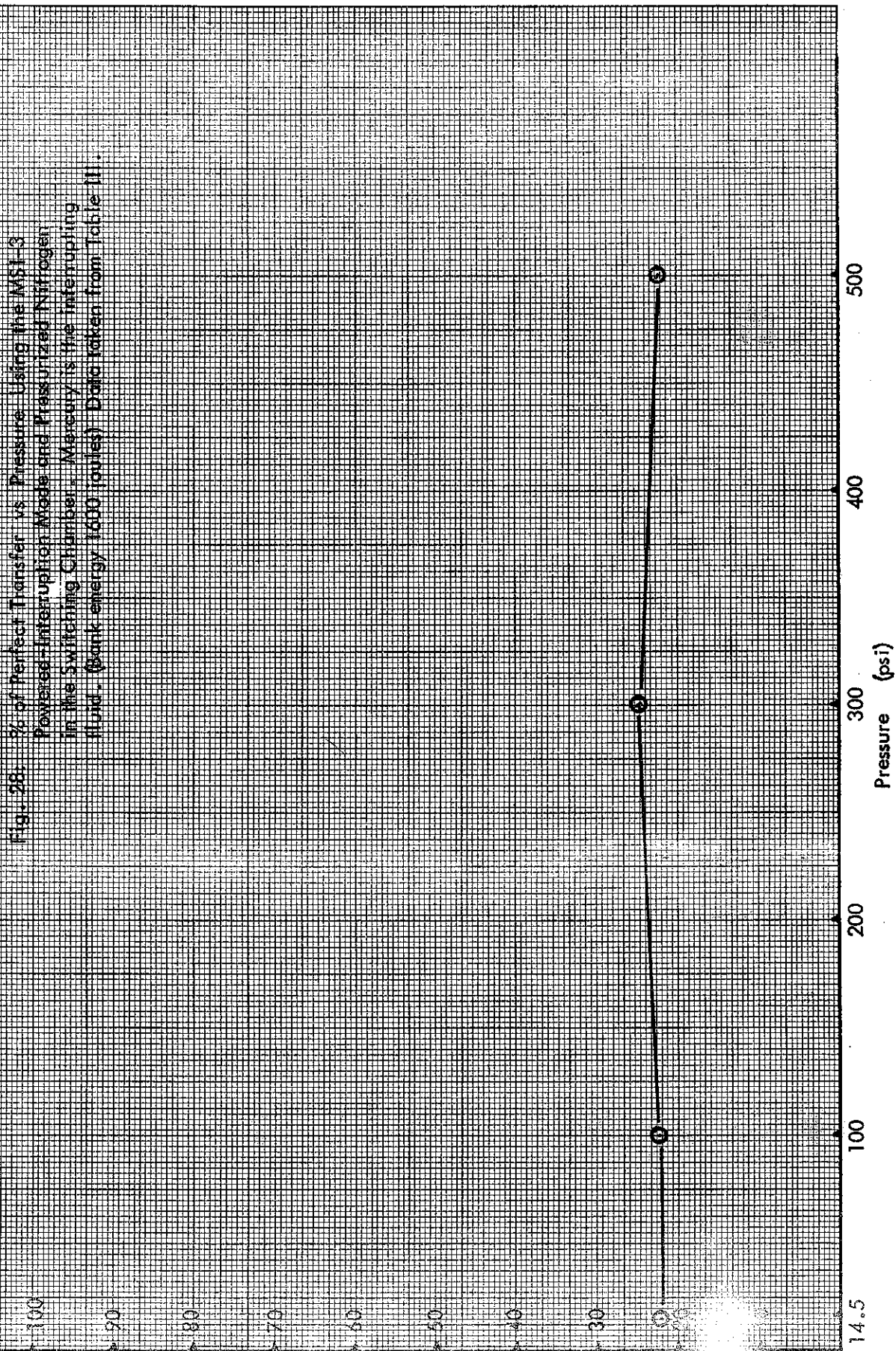
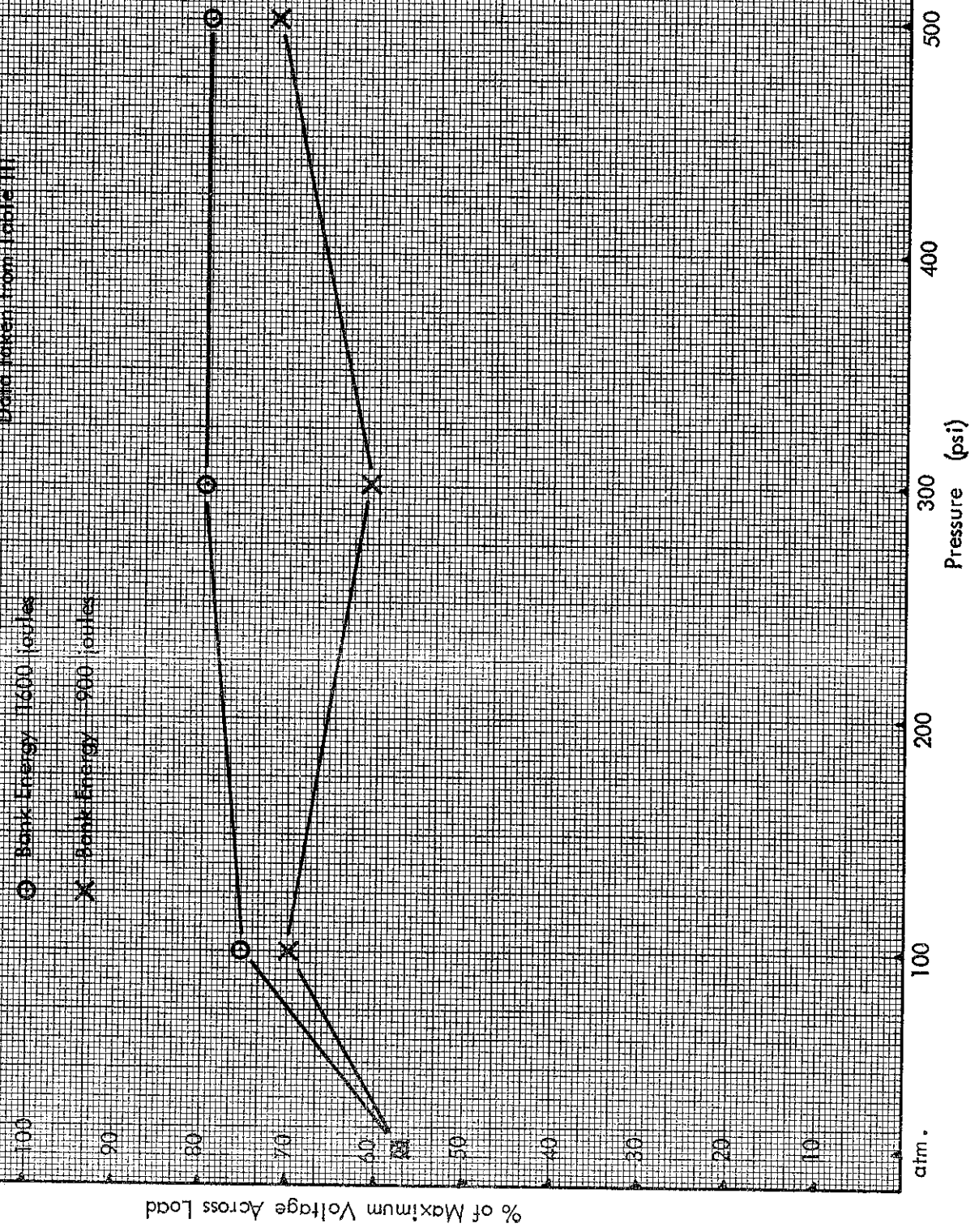


Fig. 29: % of Maximum Voltage Across Load vs. Pressure for Two Bank Energies Using the MSI-3 Powered Interruption Mode and Pressurized Nitrogen in the Switching Chamber. Mercury is the interposing fluid.
Data taken from Table III



○ Bank Energy 1600 joules

× Bank Energy 900 joules

% of Maximum Voltage Across Load

atm.

200

300

400

500

Pressure (psi)

Fig. 37: Cross-sectional Diagram of the MSI-4T

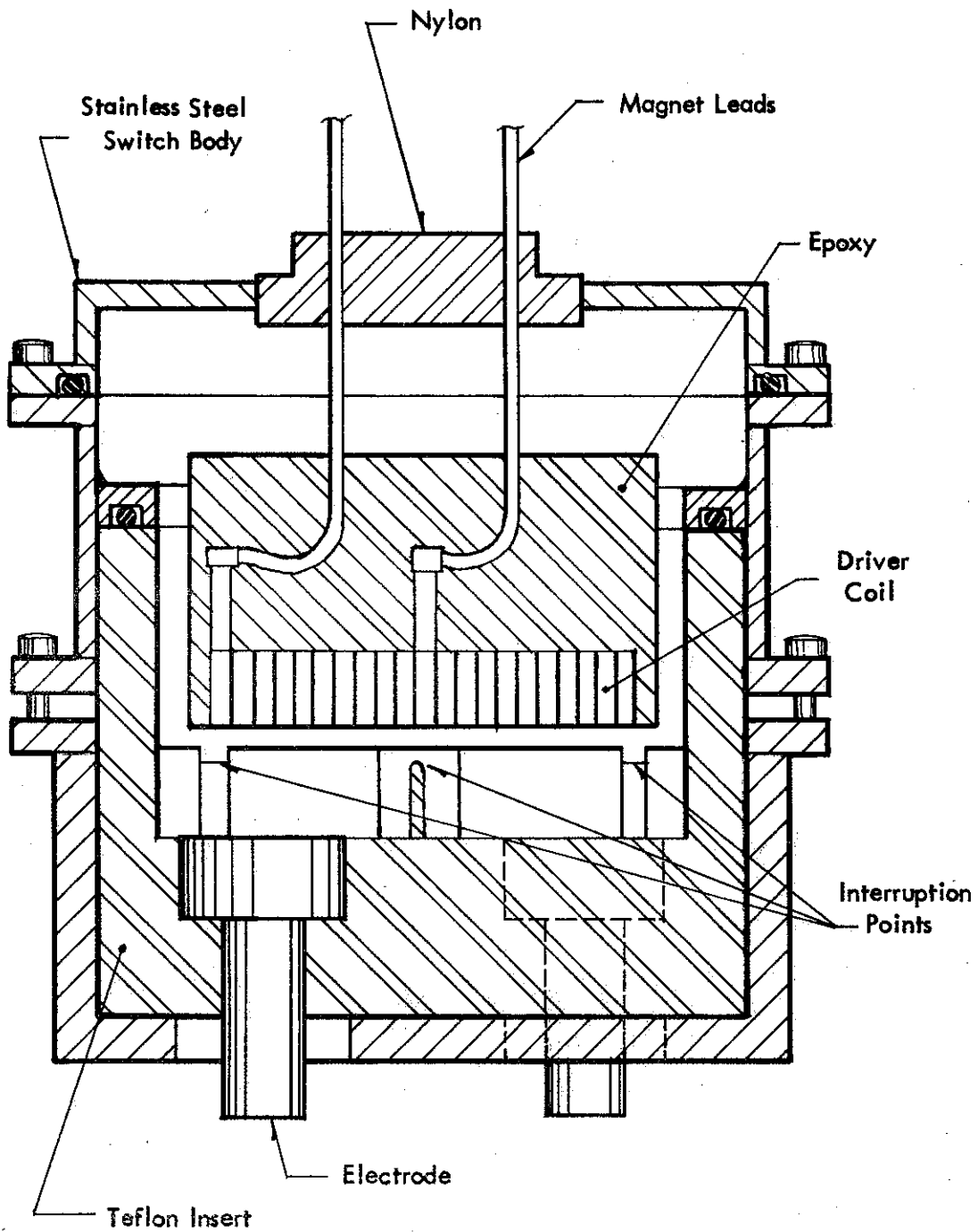
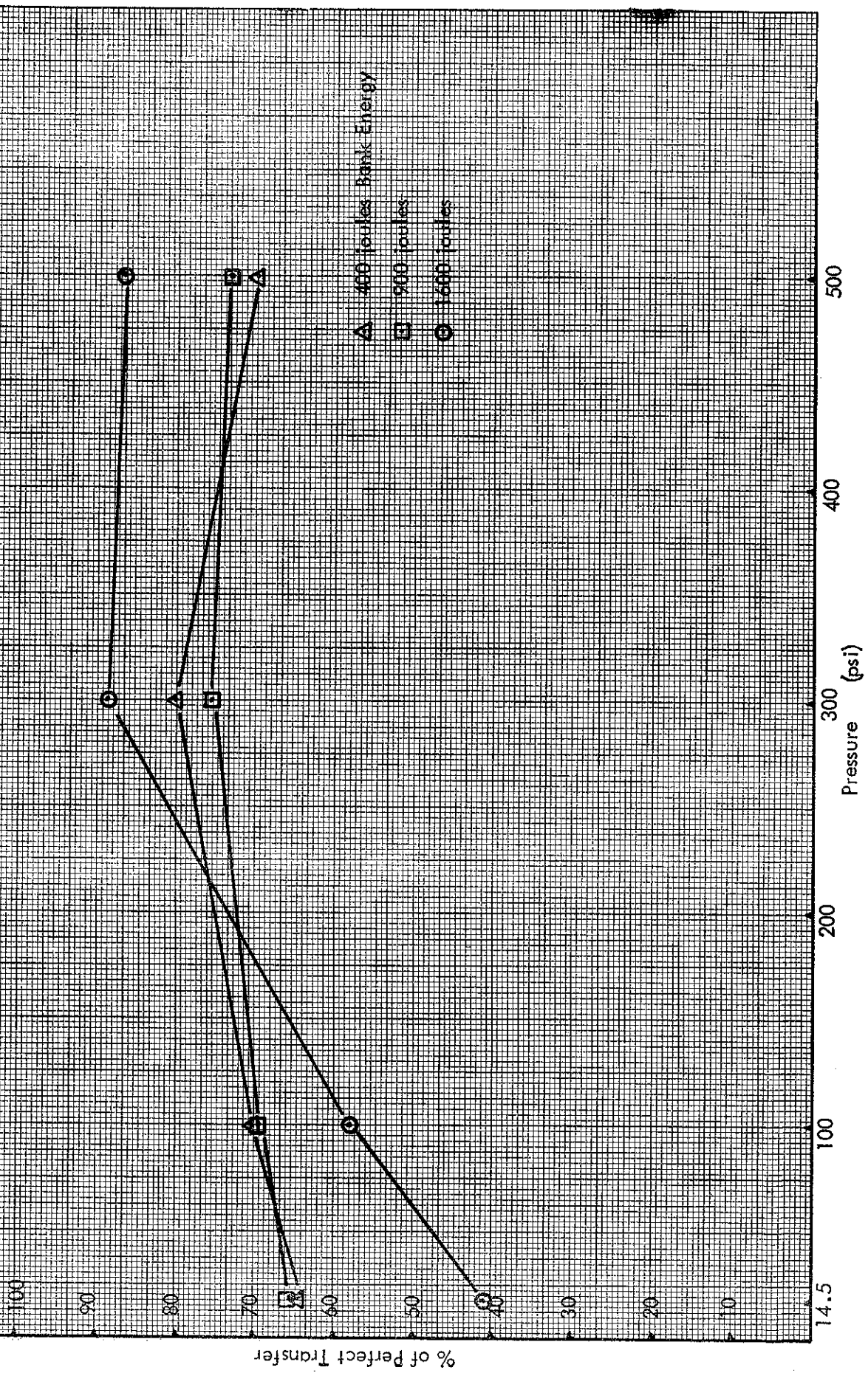


Fig. 38: % of Perfect Transfer vs Pressure for Various Bank Energies Using the MS1-AP Powered-Intermittent Mode and Pressurized Nitrogen in the Switching Chamber. Mercury is the Interrupting Fluid. Data taken from Table IX



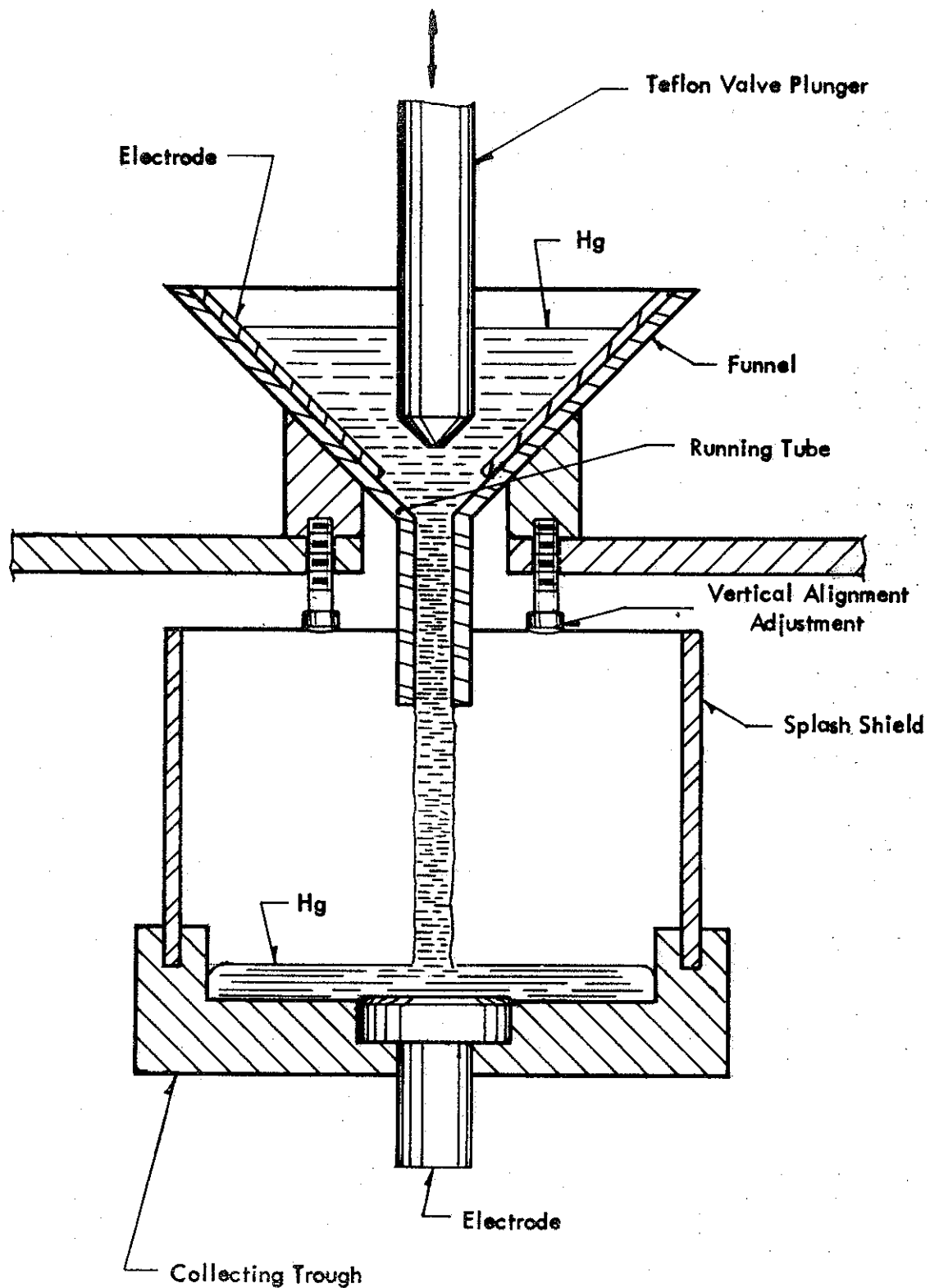


Fig. 39: The Columnar Vertical Flow Interrupter (CVFI)

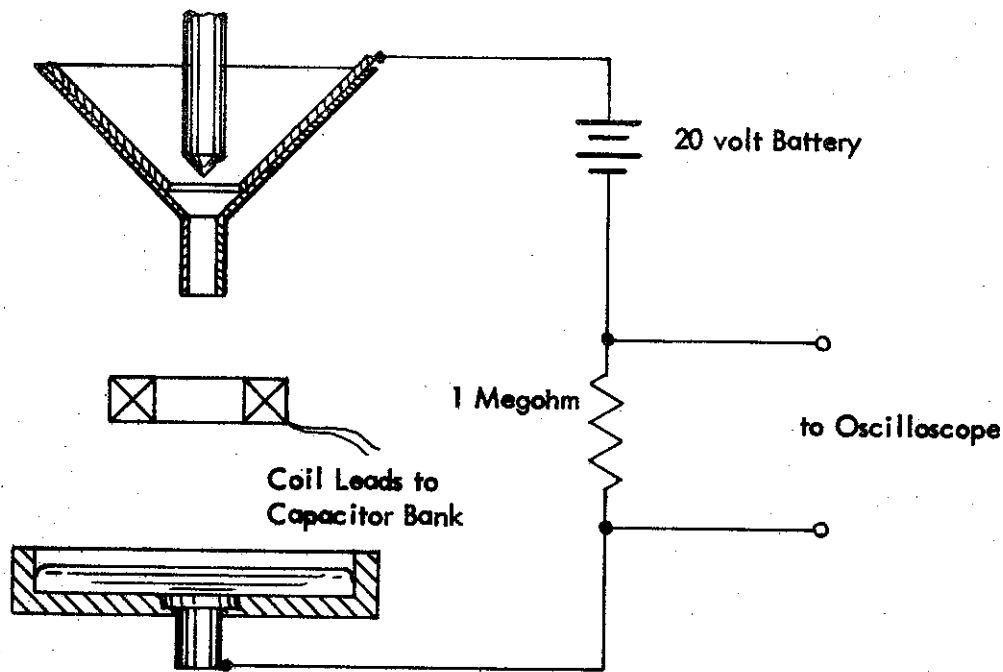


Fig. 40: Circuitry for Preliminary Testing of the CVFI
 Interruptions are not assisted by self-interruption forces since current through column is $\approx 20 \mu$.

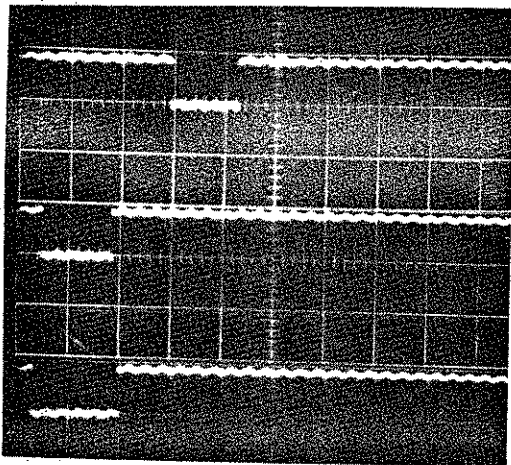


Fig. 41:
 Voltage across the 1 megohm resistor shown above. Shots are taken at various bank voltages, all at 50 msec/cm; 20 v/cm. When trace is on center grid line, switch is open.

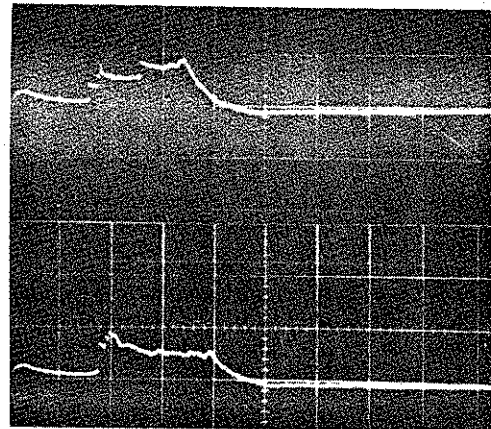


Fig. 42:
 Example of Self-Interruption and Powered-Interruption with Pancake Type Coil.
 Top: Coil energized (30 μ f - 6 kv)
 Bottom: Self-interruption
 5 msec/cm; 100 v/cm
 IND-1 charged from 800 μ f - 2kv.

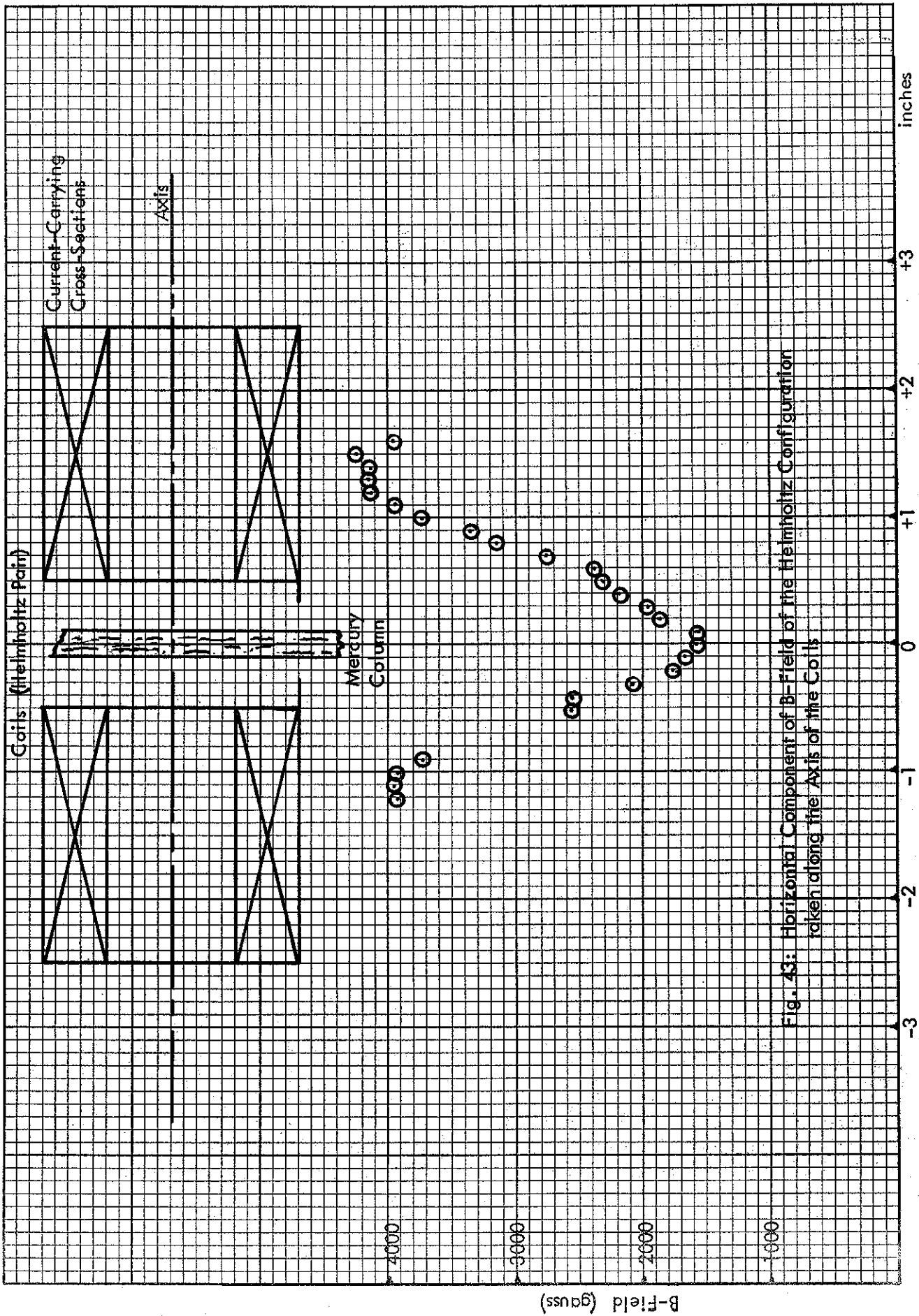


Fig. 43: Horizontal Component of B-Field of the Helmholtz Configuration taken along the Axis of the Coils

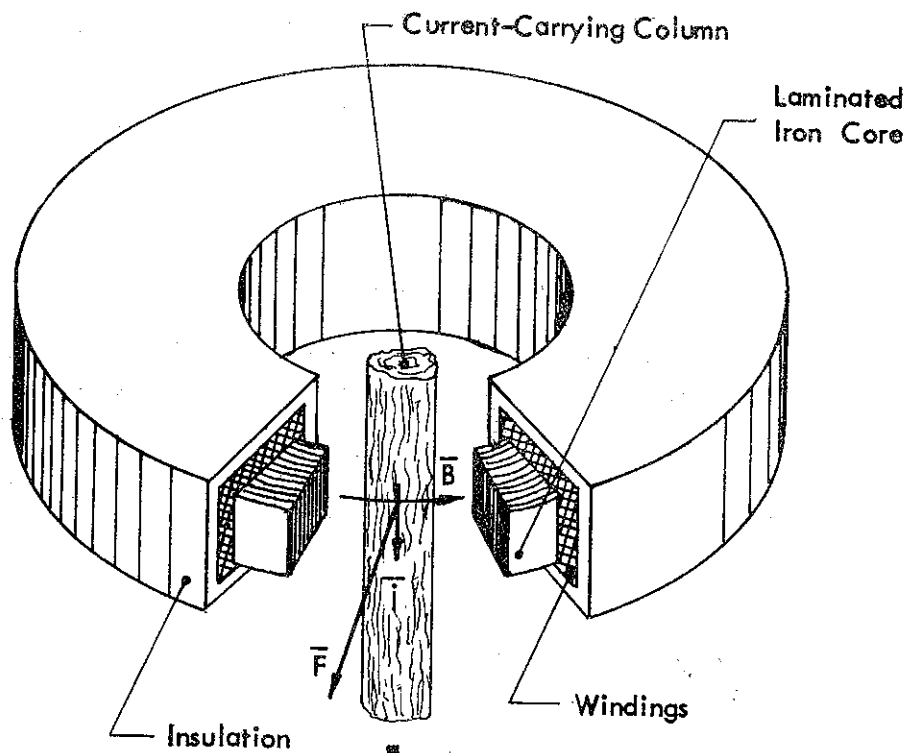


Fig. 44: The C-90 Coil. The $\vec{j} \times \vec{B}$ force is directed radially outward from the center of the toroid.

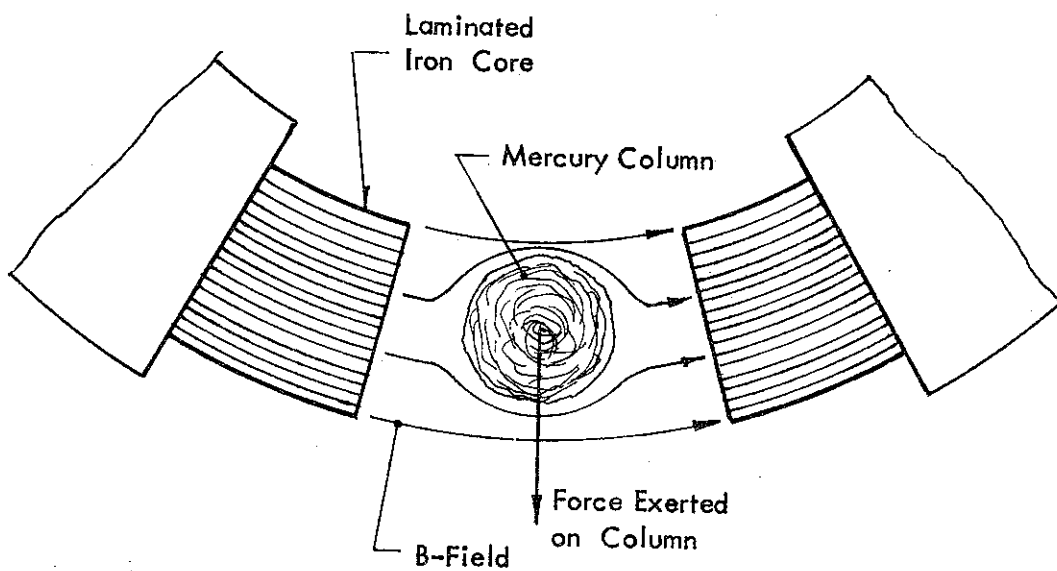


Fig. 45: Field Geometry Produced by the C-90 Coil

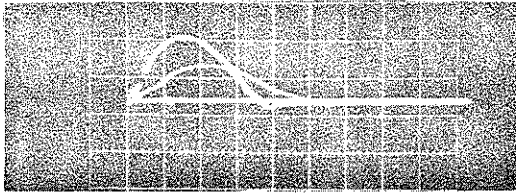
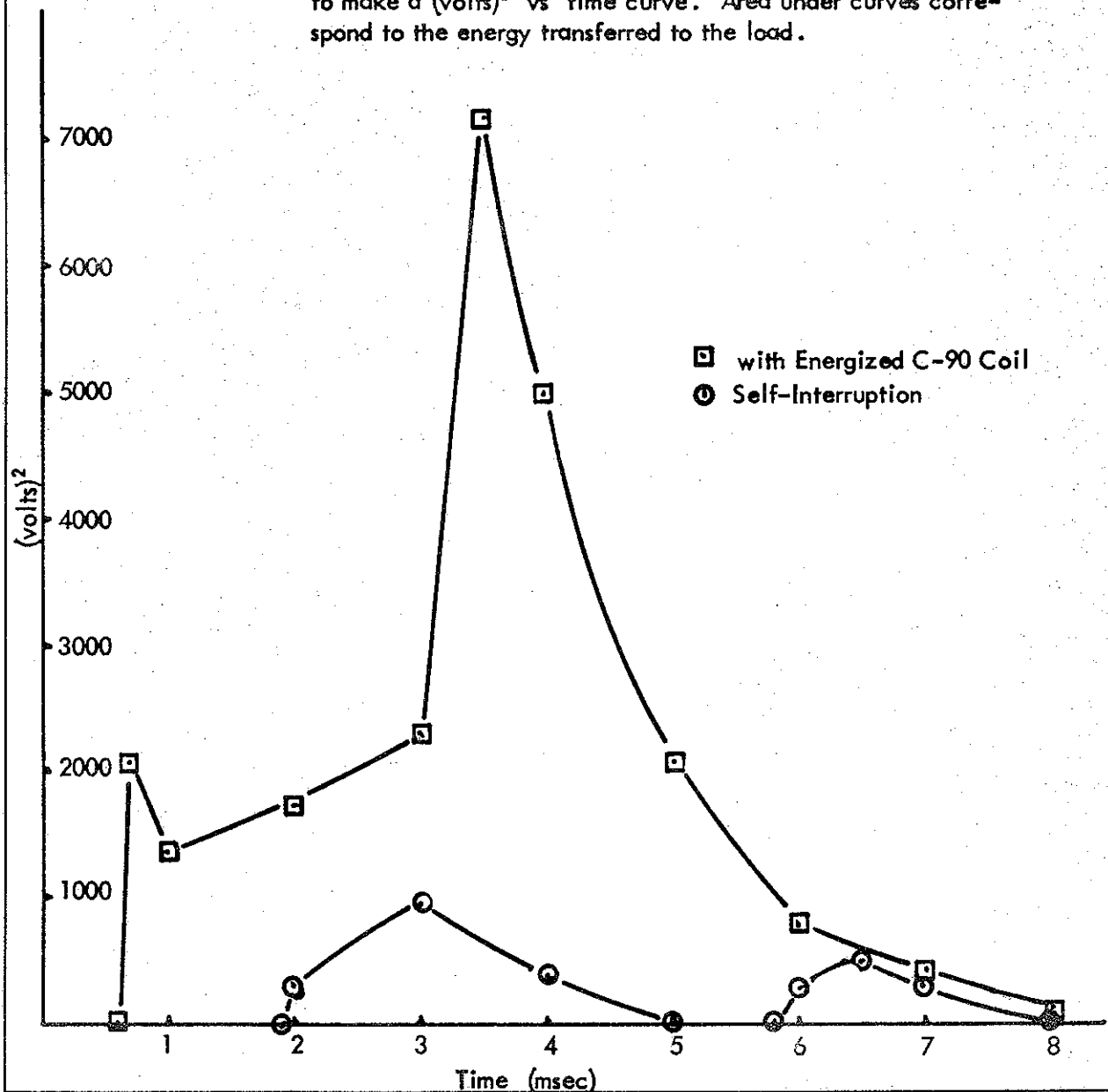


Fig. 46: B-Field Pickup in Gap of C-90 Coil. Oscillogram shows only 1/2 cycle since ignitron cuts off. 50 μ sec/cm

Fig. 47: Interruption Produced by Self-Interruption and an Energized C-90 Coil. Voltage shown on an oscillogram was transcribed to make a (volts)² vs time curve. Area under curves correspond to the energy transferred to the load.



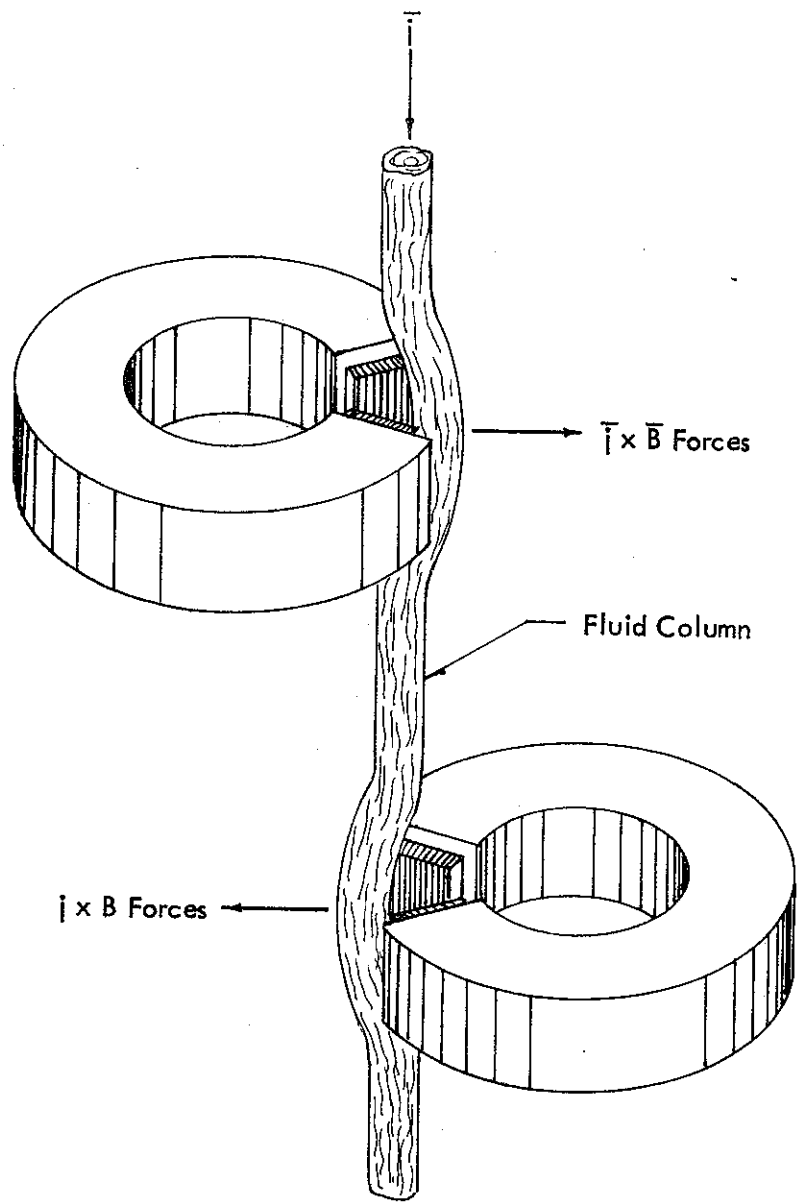


Fig. 48: Double C-Core Experimental Configuration Showing the Forces Exerted on the Mercury Column. For clarity the coils are shown much farther apart than is the actual case.

